Developmental Biology 475 (2021) 91–105

Contents lists available at ScienceDirect

Developmental Biology

journal homepage: www.elsevier.com/locate/developmentalbiology

A conserved role for *arrow* in posterior axis patterning across Arthropoda

Emily V.W. Setton *, Prashant P. Sharma **

Department of Integrative Biology, University of Wisconsin-Madison, Madison, WI, USA 53706

ARTICLE INFO

Keywords:
Wingless
Teloblastic growth
Gene regulatory network
Body plan

ABSTRACT

Segmentation is a key characteristic of Arthropoda that is linked to the evolutionary success of this lineage. It has previously been shown in both vertebrates and short germ insects that posterior segmentation requires canonical Wnt (cWnt) signaling, which maintains the expression of Caudal and the posterior growth zone; disruption of cWnt signaling incurs posterior truncations in these lineages due to the loss of the tail bud. However, comparable datasets for Wnt signaling are limited outside of holometabolous insects, due to incomparable phenotypic spectra and inefficacy of gene misexpression methods in certain model species. We applied RNA interference (RNAi) against the Wnt co-receptor *arrow* (*arr*), a key member of the cWnt signaling pathway in holometabolous insects and vertebrates, to examine posterior axis elongation of the cobweb spider *Parasteatoda tepidariorum* (short germ embryogenesis; one *Wnt8* homolog), the cricket *Gryllus bimaculatus* (intermediate germ; one *Wnt8* homolog), and the milkweed bug *Oncopeltus fasciatus* (short germ; two *Wnt8* homologs). Knockdown of *arr* in insects resulted in posterior truncations affecting the gnathos through the abdomen in *O. fasciatus*, whereas posterior truncations only affected the T3 segment through the abdomen in *G. bimaculatus*. Spider embryos with disrupted *arr* expression exhibited defects along the entire axis, including segmentation defects throughout the germband. RNA-Seq-based differential gene expression analysis of severe *Ptep-arr* loss-of-function phenotypes at two developmental stages was used to confirm that knockdown of *Ptep-arr* results in systemic disruption of the Wnt pathway. Intriguingly, we found that knockdown of *arr* did not abrogate *Wnt8* expression in any of the three species, with *cad* expression additionally retained in severe loss-of-function phenotypes in the cricket and the spider. Together with data from a holometabolous insect, our results suggest that cWnt signaling is not required for maintenance of *Wnt8* expression across Arthropoda. These outcomes underscore the diagnostic power of differential gene expression analyses in characterizing catastrophic phenotypes in emerging model species.

1. Introduction

The segmented body plan of arthropods and its ensuing modularity is linked to the evolutionary success of this phylum (Cisne 1974). The gene regulatory network (GRN) underlying segmentation is best understood in the fruit fly *Drosophila melanogaster*. The canonical arthropod segmentation cascade begins with maternal coordinate genes, with sequential activation of gap genes, pair rule genes, and segment polarity genes. While mechanistically well circumscribed, segmentation in *Drosophila melanogaster* constitutes a derived condition (long germ embryogenesis), whereas most arthropods undergo short germ development, which comprises a *Drosophila*-like mechanism in the anterior end (simultaneous formation of segments) and a vertebrate-like mechanism in the posterior (sequential addition of segments from a posterior growth zone; Liu and Kaufman 2005; Clark 2017).

In short germ arthropods, canonical Wnt signaling is understood to be necessary for the maintenance of posterior growth and the tail bud, via maintenance of Caudal (Cad) (Mcgregor et al., 2008; Chesebro et al., 2013). Canonical Wnt (cWnt) signaling is typically defined by dependence on the β-catenin intermediary to transduce Wnt signal, and consists of the Wnt binding to its receptor, a Frizzled (Fz) family gene product, and its co-receptor Arrow (Arr; vertebrate homologs: LRP5 and LRP6). The presence of a Wnt transduces a signal to, and recruits, Disheveled and Axin to cell surface receptors (Wehrli et al., 2000; Baig-Lewis et al., 2007; Zeng et al., 2007; Cadigan and Waterman 2012). The movement of Axin to the cell membrane via Arr activity inhibits the Shaggy (Sgg; vertebrate homolog: GSK-3) destruction complex, allowing Armadillo (β-catenin) to avoid degradation, enter the nucleus, and begin transcription of genes under control of Pangolin (Pan; vertebrate homolog: TCF) (Tolwinski et al., 2003; Logan and Nusse 2004; Cadigan and Liu 2006;

* Corresponding author.;
** Corresponding author.
E-mail addresses: setton@wisc.edu (E.V.W. Setton), prashant.sharma@wisc.edu (P.P. Sharma).

https://doi.org/10.1016/j.ydbio.2021.02.006
Received 4 July 2020; Received in revised form 10 February 2021; Accepted 11 February 2021
Available online 16 February 2021

Peterson-Nedry et al., 2008; Cadigan and Waterman 2012; Lybrand et al., 2019). Targets of Wnt signaling include some members of the aforementioned pathway, thus creating a feedback loop.

Disruption of *cad* expression results in truncation of posterior segments and abrogation of the tail bud in several posteriorly segmenting insects and one crustacean, and *cad* is required for regulation of pair rule segmentation genes (Copf et al., 2004; Shinmyo et al., 2005; Chesebro et al., 2013; El-Sherif et al., 2014). Intriguingly, vertebrate *cad* homologs (*Cdx*) are similarly controlled by Wnts during somitogenesis, and *Cdx* depletion also results in posterior (tail) truncations, segmental defects, and misregulation of posterior Hox genes (Isaacs et al., 1998; Ehrman and Yutzey 2001; van den Akker et al., 2002; Chawengsaksophak et al., 2004; Shimizu et al., 2005). For posterior segment-forming phyla, terminal segmentation resulting from Wnt-Cad signaling was previously reconstructed to be an ancestral condition in Bilateria (Copf et al., 2004; Martin and Kimelman 2009), though recent work in hemichordates has suggested that the ancestral function of Wnt signaling in the posterior terminus may instead have been axis elongation, with subsequent and independent co-option events giving rise to segmented bauplans (Fritzenwanker et al., 2019).

Within arthropods, functional data on the Wnt gene family are nevertheless largely restricted to two holometabolous insect models, the fruit fly *Drosophila melanogaster* and the flour beetle *Tribolium castaneum*. As *D. melanogaster* exhibits long germ embryogenesis, a derived mode of segmentation restricted to some insect groups, *T. castaneum* often serves as the archetype of the ancestral segmentation mode for the arthropods (i.e., short germ embryogenesis). Comparative data outside insect models remain scarce (e.g., Stollewerk et al., 2003; Chipman et al., 2004; Angelini and Kaufman 2005; Mcgregor et al., 2008; Auman and Chipman 2018), with functional datasets especially ambiguous with regard to the conserved aspects of Wnt activity across arthropods. As one example, *wingless* (*Wnt1*) is regarded as a classic segment polarity gene and has been broadly surveyed across model and non-model arthropods (e.g., Hughes and Kaufman 2002; Inoue et al., 2002; Damen 2007; O'Donnell and Jockusch 2010; Auman and Chipman 2018). But RNAi-mediated knockdown of insect *wg* homologs has been met with variable—and often incomparable—results. RNAi against *wg* in *T. castaneum* and the water strider *Limnoporus dissortis* causes truncated appendages and disruption of segmentation boundaries across all tagmata (Ober and Jockusch 2006; Bolognesi et al., 2008a; Refki and Khila 2015), but not truncation of the AP axis. *wg* RNAi in the cockroach *Periplaneta americana* truncates posterior segments—an effect linked to the requirement of *wg* for activation of *cad* in this species, but the effect of *wg* knockdown on cockroach appendages was not assessed (Chesebro et al., 2013). RNAi against the *wg* ortholog of the milkweed bug *Oncopeltus fasciatus* has no discernible effect on appendages, with AP segmentation defects limited to partial segmental fusions along the dorsum of some abdominal segments (Angelini and Kaufman 2005). Attempts to knock down *wg* in the cricket *Gryllus bimaculatus* resulted in only wild type hatchlings, a result shown to be attributable to very transient diminution of *wg*, with subsequent recovery of expression (Miyawaki et al., 2004). In cases where the strength of the knockdown was not reported, it is difficult to assess whether these differences reflect evolutionary lability, functional redundancy among the Wnts, or variability in experimental efficiency.

Functional data for Wnt homologs are even further limited outside of Hexapoda and relatively little is known about cWnt signaling in Chelicerata, the sister group to the remaining arthropods, beyond homolog incidence and purely descriptive gene expression data. It has previously been shown that *Wnt8* is required for proper formation of the posterior growth zone in the spider *Parasteatoda tepidariorum* and acts to maintain the expression of *cad*; RNAi against spider *Wnt8* results in the truncation of all opisthosomal (abdominal) segments, whereas anterior segments are not affected (Mcgregor et al., 2008). This result closely parallels the phenotypes observed upon RNAi against *Wnt8* in *T. castaneum* (Bolognesi et al., 2008a) and against *wg* in *P. americana* (Chesebro et al., 2013). No other functional data are available for Wnt homologs in Chelicerata, largely due to lack of success in generating phenotypes via RNAi (in our hands, outcomes have been similar to those described in the cricket *G. bimaculatus* by Miyawaki et al., 2004).

An alternative approach to disrupting cWnt signaling efficiently may be targeting the co-receptor *arr*, which is critical to Wnt signal transduction (Baig-Lewis et al., 2007; Wehrli et al., 2000). Within arthropods, loss-of-function (LOF) phenotypes for *arr* were previously limited to *D. melanogaster* and *T. castaneum*. In *D. melanogaster*, *arr* LOF mutants exhibit a segment polarity phenotype comparable to *wg* LOF mutants (Wehrli et al., 2000). It was also shown that while *arr* mutants exhibited the effects of inhibited Wg signaling, the Wg ligand was nevertheless produced, suggesting that *arr* is downstream of Wnt signaling (Wehrli et al., 2000). Effects of RNAi against *arr* in *T. castaneum* ranged from complete inhibition of segmentation (in tandem with loss of *wg* and Engrailed expression) to truncation of subsets of posterior segments (Bolognesi et al., 2009). This result parallels the function of the vertebrate homolog LRP6; in *Mus musculus*, LRP6 has been shown to be necessary for transducing the signal of several Wnts and the loss-of-function phenotype includes truncation of tail vertebrae, neural tube defects, and limb malformation (Pinson et al., 2000).

We recently performed RNAi against the *arr* homolog of *P. tepidariorum* to disrupt canonical Wnt signaling and test the requirement of Wg signaling for appendage development (Setton and Sharma 2018). The severe phenotype class consisted of a germband that did not express *wg* or *en-1*, supporting disruption of segmentation. Assays of two head marker genes (*orthodenticle-1* and *labial-1*) suggested that the anterior end of the AP axis was nevertheless intact. As the purpose of that study was to explore appendage development, posterior axis patterning was not analyzed further.

Here, we investigated the function of *arr* homologs in three non-holometabolous arthropods: *P. tepidariorum*, *O. fasciatus* (a short germ insect), and *G. bimaculatus* (an intermediate germ insect). Given the presumed ancestral role of *Wnt8* in patterning the posterior trunk across Arthropoda through regulation of *cad* (Mcgregor et al., 2008), we queried the effect of *arr* disruption on the expression of *Wnt8* and *cad* homologs of the three species. Leveraging genomic tools in *P. tepidariorum*, we implemented differential gene expression (DGE) analysis in conjunction with traditional gene expression assay methods to quantify the effects of disrupting *arr* on axis-forming pathways.

2. Methods

2.1. Bioinformatics, sequencing, and phylogenetic analysis

Sequences previously generated or compiled by us (Setton and Sharma 2018) were used to test orthology of arthropod *arr* homologs. Additional orthologs of LRP gene family members were identified in the genome of *Oncopeltus fasciatus* (Panfilio et al., 2019), as well as a transcriptome of *Gryllus bimaculatus* sequenced herein from a range of embryonic stages, using procedures detailed in our previous works for library preparation and assembly (Sharma et al., 2014; Ballesteros and Sharma 2019). For all searches, *D. melanogaster arr* (NP_524737.2) was initially used as the peptide sequence query in tBLASTn searches, and hits with e-value $< 10^{-5}$ were retained. All putative orthologs were verified using reciprocal BLAST searches. Multiple sequence alignment was conducted *de novo* with MUSCLE v.3.8.31 (Edgar 2004). Outgroup sequences used to root the tree consisted of LRP4 orthologs and a *D. melanogaster megalin* sequence. Phylogenetic reconstruction of amino acid alignments consisted of maximum likelihood analysis with RAxML v.8.0 (Stamatakis 2014) under the LG + Γ model, with 250 independent starts and 500 bootstrap resampling replicates (following the model selection strategy in Setton and Sharma 2018). The same set of approaches was undertaken for generating gene trees for *frizzled* and Wnt gene families. Alignments and annotated tree files are available as supplementary material. Raw sequence reads from RNA-seq experiments are deposited in NCBI Sequence Read Archive (PRJNA701472).

2.2. Cloning of orthologs and probe synthesis

Fragments of *Ptep-arr*, *Ofas-arr*, and *Gbim-arr* were amplified using standard PCR protocols and cloned using the TOPO® TA Cloning® Kit with One Shot® Top10 chemically competent *Escherichia coli* (Invitrogen, Carlsbad, CA, USA) following the manufacturer's protocol, and their PCR product identities were verified via sequencing with M13 universal primers. All gene-specific primer sequences are provided in Table S1.

2.3. Embryo collection, fixation, in situ hybridization, fluorescent immunohistochemistry, and imaging

Animals were maintained, and embryos fixed and assayed for gene expression, following established or minimally modified protocols, as detailed previously (Donoughe and Extavour 2016; Setton et al., 2017; Setton and Sharma 2018). PCRs for generating riboprobe templates, synthesis of DIG-labeled probes, and preservation of embryos all followed our recently detailed procedures (Setton and Sharma 2018). Probes were used at a concentration of 30–50 ng/μl. Sense probes were always developed for the same duration as complementary antisense probes. Completion of staining lasted 0.5–8 h at room temperature. Whole mount images were taken using a Nikon SMZ25 fluorescence stereomicroscope mounted with a DS-Fi2 digital color camera driven by Nikon Elements software. Fluorescent immunohistochemistry was performed following established procedures (Schwager et al., 2015) with primary antibodies for rabbit anti-phospho-histone H3 (ThermoFisher, Waltham, MA) 1:500 and conjugated horseradish peroxidase (Alexa Fluor 647) 1:200 (Jackson ImmunoResearch). Secondary antibodies were goat anti-rabbit (Alexa Fluor 594) 1:200 (Thermofisher). Confocal microscopy was performed with a Zeiss LSM 710 driven by Zen software. Imaging analysis was performed using inbuilt tools in ImageJ2 (Rueden et al., 2017) and Fiji (Schindelin et al., 2012). Time lapse videos were taken for spider embryos affixed to glass slides under halocarbon-700 oil (Sigma Aldrich). Images were captured every 30 min using the Nikon SMZ25 stereomicroscope, for the duration of embryogenesis. Video compilation and annotation was performed using Fiji.

2.4. Double-stranded RNA synthesis and maternal RNA interference

Double-stranded RNA (dsRNA) was synthesized following the manufacturer's protocol using a MEGAscript® T7 kit (Ambion/Life Technologies, Grand Island, NY, USA) from amplified PCR product. dsRNA quality was checked and concentration adjusted to 2.5 μg/μl. For spiders, RNAi was performed with 20 μg of dsRNA delivered over eight days to 27 virgin females (another 17 for negative control injections), and embryos were collected from cocoons 2–5 as previously described by us (Setton and Sharma 2018). Negative controls with injected with an equal volume of deionized water, following Pechmann et al. (2017). For *O. fasciatus*, 10 μg of dsRNA was delivered as a single injection to 19 anesthetized virgin females (another six females for negative control injections), following our previous procedures (Setton et al., 2017). For *G. bimaculatus*, 33 μg of dsRNA was delivered as a single injection to anesthetized seven virgin females (another three females for negative control injections) using a fine syringe immediately posterior to the T3 coxa, following established protocols in this system (Shinmyo et al., 2005). For both species, egg clutches 2–8 were collected and scored, and negative controls were injected with an equal volume of 1 × *Tribolium* injection buffer. To rule out off-target effects, dsRNA was synthesized for injection as two non-overlapping fragments of similar size in each species (Fig. S1; Table S2).

2.5. qPCR

First-strand cDNA was prepared using oligo(dT) primers and SuperScript III reverse trancriptase (ThermoFisher) from negative controls and knockdown embryos at 48 h after egg-laying (hAEL) for *O. fasciatus*; late egg stage 6 (*sensu* Donoughe and Extavour 2016; corresponding to germband elongation stage) for *G. bimaculatus*; and when the oldest RNAi phenotypes in a given cocoon resembled germbands in *P. tepidariorum* (7 days). For comparison, wild type embryos of equal age (stage 14, ventral closure stage) were sampled. Additional samples of *P. tepidariorum* were collected from cocoons of uninjected females at stages 6 (dorsal field stage), 7 (germband stage), and 8 (prosomal limb bud stage), following the staging system of Mittmann and Wolff (2012). Samples were selected from clutches displaying strong phenotypic penetrance for insect models and chosen through visual inspection for spider RNAi experiments. Three to four technical replicates were run for every analysis using PowerUp SYBR Green Master Mix (Life Technologies) on a StepOne Plus Real-Time PCR instrument (Applied Biosystems) following the manufacturer's protocol. Results were analyzed using StepOne Plus software (Applied Biosystems). The housekeeping gene eukaryotic translation release factor-3 was used for normalization for both insects, whereas α-tubulin was used for spiders (Table S1).

2.6. Differential gene expression analysis

Three sets of biological replicates for *Ptep-arr* RNAi embryos and negative controls were assembled at two different time points during embryogenesis (120 and 144 hAEL). Each experimental sample contained 18–60 embryos from the same cocoon, selected to reflect the most severe end of the phenotypic spectrum in the knockdown experiments (Fig. S1; Tables S2, S3). Total RNA was extracted from whole embryos using TRIzol Tri Reagent (Thermofisher), following the manufacturer's protocol. and libraries prepared for sequencing using standard protocols for the Illumina HiSeq 2500 platform with a 1 × 100 SE sequencing strategy. Multiplexing was arranged to recover an expected 20 M reads per library. Adaptor removal and quality trimming was performed with Trimmomatic v 0.35 (Bolger et al., 2014) prior to analysis. Reads were mapped to the *P. tepidariorum* genome (Schwager et al., 2017) using the density of reads mapped to the genome as a proxy for transcript abundance, as implemented by salmon v. 0.9.1 under default parameters (Patro et al., 2017). Differential gene expression analysis was performed using DESeq2 v. 1.14.1 (Love et al., 2014).

3. Results

3.1. RNAi against hemimetabolous insect arr homologs

To establish the degree of conservation of *arr* function in insects, we performed maternal RNAi against *arr* homologs in two hemimetabolous species: the milkweed bug *Oncopeltus fasciatus* and the two-spotted cricket *Gryllus bimaculatus*. The homolog of *arr* was discovered in the genome project of *O. fasciatus* (Panfilio et al., 2019). However, we were not able to discover a sufficiently large fragment of the *arr* homolog in the available transcriptomic resources of *G. bimaculatus*; only a 604-bp fragment was discovered in an older Newbler assembly of 454 reads (isotig16545; Zeng and Extavour 2012). To obtain a large sequence for *arr* in *G. bimaculatus*, as well as enhance genomic resources for this model system, we generated a paired end reference transcriptome using a range of embryonic stages and sequenced these data on an Illumina HiSeq 2500 platform, following our previously described procedures (Sharma et al., 2014; Ballesteros and Sharma 2019). Orthology of *arr* homologs was verified using multiple sequence alignment and gene tree analysis under maximum likelihood (Fig. S2; Setton and Sharma 2018).

In the milkweed bug (Fig. 1), RNAi against *Ofas-arr* yielded a homogenous phenotypic class consisting of a rudimentary head that included the eyes, antennae, and possibly the appendage-less intercalary (third head) segment; the remainder of the AP axis was truncated (n = 842) (Fig. 1B and F). This phenotype broadly resembles its *T. castaneum* counterpart, previously described as a rudimentary head (Bolognesi et al., 2009). Injection of a smaller amount of *Ofas-arr* dsRNA (2 μg, instead of 10 μg dsRNA for the main RNAi experiments) did not

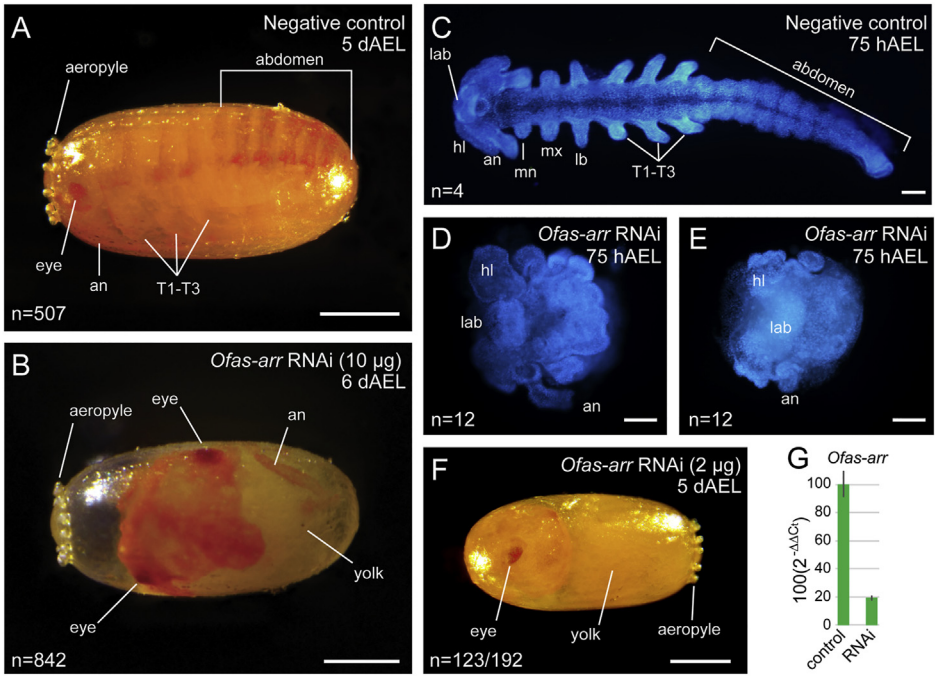

Fig. 1. RNAi against *Ofas-arr* recapitulates the *arr* knockdown phenotype reported for holometabolous insects. (A) Negative control embryo at 6 days after egg laying. Thoracic appendages and abdominal segments are readily visible. (B) *Ofas-arr* RNAi embryo at 6 days after egg laying, showing retention only of some head structures. (C) Negative control embryo stained for Hoechst at 75 hAEL showing wild type development of trunk segments. (D, E) *Ofas-arr* RNAi phenotypes exhibit developmental failure of gnathal, thoracic, and abdominal segments by 75 hAEL. Embryos are truncated after anterior-most head segments, with only the malformed head lobes, labrum, and antennae as morphological landmarks. (F) *Ofas-arr* RNAi embryos also exhibit development on the opposite side of the egg as the aeropyles (G) qPCR-based validation of *Ofas-arr* knockdown. Abbreviations: lab: labrum; an: antenna; mn: mandible; mx: maxilla; lb: labium; T1: first thoracic appendage. Scale bars: 200 µm in (A, B, F); 100 µm in (C, D, E).

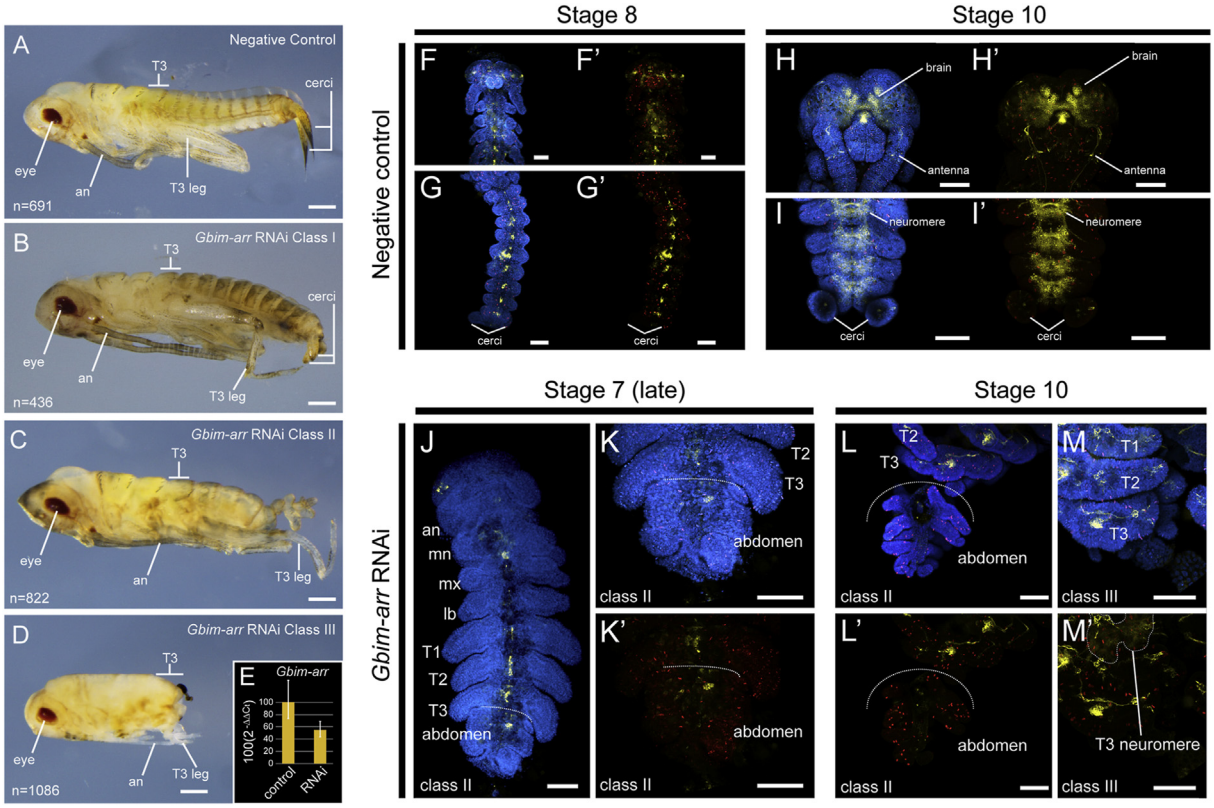

Fig. 2. RNAi against *Gbim-arr* incurs posterior segmentation defects. (A) Negative control embryo control at egg stage 23 exhibiting wild type morphology of cerci, abdominal segments, and appendages. (B) Class I (mild) phenotype of *Gbim-arr* RNAi exhibiting abnormal development of the cerci and the posterior-most abdominal segments. (C) Class II (moderate) phenotype of *Gbim-arr* RNAi exhibiting deletion of several abdominal segments and misshapen posterior tail bud. (D) Class III (severe) phenotype of *Gbim-arr* RNAi exhibiting loss of all abdominal segments and reduction of appendage size. Black staining in tail bud indicates necrosis. (E) qPCR-based validation of *Gbim-arr* knockdown. (F–L) Characterization of segmental defects using immunohistochemical staining for the neurogenic marker horseradish peroxidase. Negative control embryos of *G. bimaculatus* exhibiting wild type neurogenesis of the head (F, H) and abdomen (G, I) at egg stages 8 (F, G) and 10 (H, I). (J–M) *Gbim-arr* RNAi embryos at comparable stages exhibit truncation of the central nervous system in abdominal segments in class II (J–L) and class III (M) phenotypes. (K) Same embryo as (J) showing magnification of posterior terminus. (F′-M′) Same as (F–M) without Hoechst layer. Anterior is to the left in (A–D), up in (F–M). Scale bars are 200 µm. Scale bars: 200 µm in (A–D); 100 µm in (F–M). Abbreviations as in Fig. 1.

significantly lessen the severity of the phenotype or duration of phenotypic penetrance (Fig. S3). In addition, embryos frequently developed on the incorrect end of the egg, with the head developing opposite the aeropyles (egg spiracles) (n = 123/192 in 2 μg dsRNA experiments; Fig. 1F, Fig. S3). qPCR analysis of *Ofas-arr* expression was used to validate the knockdown in 10 μg dsRNA experiments; the reduction of expression levels was estimated to range between 79.3% and 81.8% across replicates (Fig. 1G). Similar phenotypic distributions were obtained upon knockdown of two non-overlapping fragments of *Ofas-arr* (Fig. S1).

In the two-spotted cricket, RNAi against *Gbim-arr* resulted in a range of phenotypic classes (Fig. 2). In embryos exhibiting the mildest defects (Class I phenotypes), only the cerci (terminal sensory appendages) were malformed, with up to two missing abdominal segments (n = 436; Fig. 2B). The intermediate phenotype (Class II) exhibited malformed cerci and deletion of three to nine abdominal segments; the remaining abdominal segments were often small, malformed, and twisted (n = 822; Fig. 2C). The most severe phenotypic class (Class III), demonstrated loss of all, or all but one, abdominal segments; reduction or malformation of the T3 segment; and reduction of appendages along the proximo-distal axes (n = 1086; Fig. 2D). qPCR analysis of *Gbim-arr* expression was used to validate the knockdown, whose strength was estimated to range between 31.4% and 56.3% across replicates (Fig. 2E). Similar phenotypic distributions were obtained upon knockdown of two non-overlapping fragments of *Gbim-arr* (Fig. S1).

To bridge the gap between the *T. castaneum/O. fasciatus* rudimentary head phenotype and the *G. bimaculatus* RNAi phenotypic spectrum, we assessed whether *Gbim-arr* RNAi phenotypes exhibited internal segmental defects of the anterior trunk (thorax), using fluorescent immunohistochemical staining for the central nervous system marker horseradish peroxidase (HRP) and the cell division marker phosphohistone H3 (pH3), between stages 6 and 10 (germband elongation to appendage elongation stages). Expression of HRP revealed loss of neuromeres in all abdominal segments of both Class II (n = 8) and Class III (n = 11) *Gbim-arr* RNAi embryos (Fig. 2J-M). We did not detect differences in cell division in unaffected head and thoracic segments (Fig. 2F, G, 2K, 2 L). These results support the interpretation that only a subset of segments posterior to the thorax are affected by *Gbim-arr* RNAi. The phenotypic spectrum generated here for *G. bimaculatus* thus parallels the weak *arr* knockdown phenotype in *T. castaneum* (Bolognesi et al., 2009), as well as RNAi against the *T. castaneum Wnt8* homolog (Bolognesi et al., 2008a).

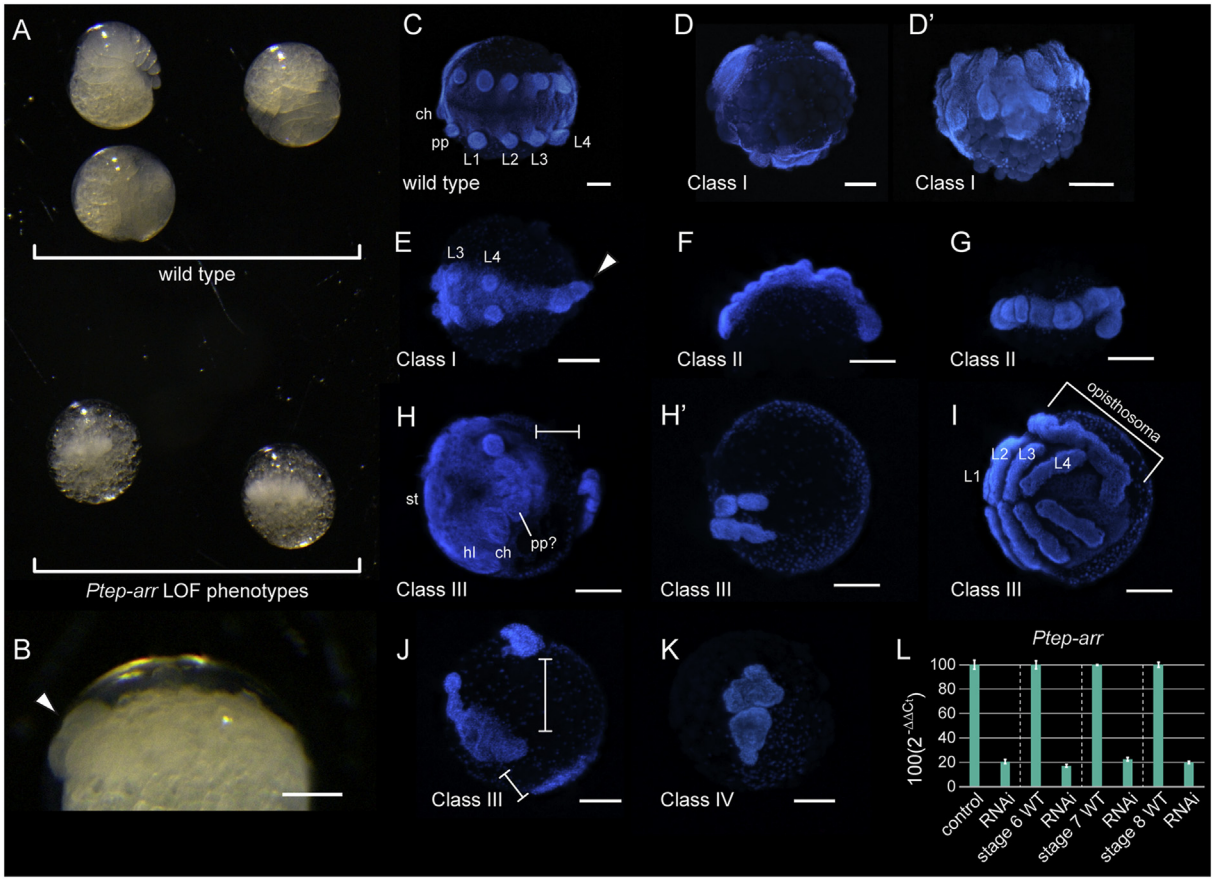

Fig. 3. RNAi against *Ptep-arr* incurs AP axis patterning and segmentation defects in the spider. (A) Bright field comparison of wild type embryos and *Ptep-arr* loss-of-function phenotype embryos of the same age. (B) Lateral view of a severe *Ptep-arr* loss-of-function phenotype. Arrowhead denotes atypical development. (C–K) Hoechst-stained *P. tepidariorum* embryos at 120–186 hAEL. (C) Negative control embryo at 120 hAEL develops to limb bud stage. (D, D′) Class I RNAi phenotype in lateral and ventral view, showing mild segmentation defects in prosomal segments at 120 hAEL. (E) Class I embryo at 186 hAEL exhibiting segmentation defects of the opisthosoma and a reduced posterior growth zone (arrowhead). (F) Lateral view of a Class II phenotype embryo at 186 hAEL exhibiting lack of appendages and irregular disposition of tissue. (G) Different Class II phenotype embryo in ventral view, with no appendages and malformed posterior terminus (comparable to embryo shown in B). (H) Anteroventral view of a Class III phenotype embryo showing recognizable head structures, followed by a lacuna in the germband (bracket). (H′) Posteroventral view of the same embryo showing delamination of putative posterior tissue. (I) Posteroventral view of another Class III phenotype embryo, showing an unaffected prosoma and a fully delaminated, unsegmented opisthosoma. (J) Class III phenotype embryo exhibiting multiple lacuna and irregularly oriented structures. (K) Class IV RNAi phenotype constituting a putative germ disc remnant. (L) qPCR-based validation of *Ptep-arr* knockdown, using as controls wild type embryos of the same age, at stage 6, at stage 7, and at stage 8. Abbreviations: ch: chelicera; hl, head lobe; pp: pedipalp; L1, first walking leg. Scale bars: 100 μm.

3.2. RNAi against spider Ptep-arr homolog

The severe *Ptep-arr* LOF phenotype is a small, nondescript germband, lacking clear morphological landmarks and exhibiting developmental arrest (Setton and Sharma 2018). We previously showed that these embryos lack expression of *wg* and *en-1*, but retain regionalized expression of the head markers *orthodenticle-1* (expression in the anterior-most pair of segments), *labial-1* (expressed in the third head segment), and the gap gene *Sp6-9* (expressed in the L1 and L2 segments; Setton and Sharma 2018). These results were previously interpreted to mean that the anterior portion of the AP axis as retained in the phenotype, comparable to the *T. castaneum* rudimentary head phenotype (Bolognesi et al., 2009). The posterior region of the spider phenotype was previously assumed to be truncated, as with spider *Wnt8* (Mcgregor et al., 2008) or *T. castaneum arr* RNAi phenotypes (Bolognesi et al., 2008a), because opisthosomal segments are formed by sequential addition of segments from the posterior growth zone in the spider. However, in contrast to the *T. castaneum* rudimentary head phenotype, no morphological landmarks were observed in the spider *arr* LOF phenotype to substantiate this interpretation.

To characterize in greater detail the spider *arr* LOF phenotype, we examined a wider spectrum of phenotypes by including later cocoons in our examination, as well as permitting a subset of RNAi embryos to develop for longer than in our previous experiments (120 and 144 hAEL in Setton and Sharma 2018). First, to rule out off-target effects, we knocked down two non-overlapping fragments of *arr* in *P. tepidariorum* and confirmed the same range of phenotypes between fragments (n = 1353) (Fig. S1; Table S3). Second, we repeated this experiment to classify the ensuing phenotypic spectrum after excluding dead, indeterminate (i.e., broken), and wild type embryos, and retaining only *Ptep-arr* LOF phenotype embryos (n = 316).

In embryos exhibiting the mildest phenotypes (Class I; n = 69/316), a germ band presenting recognizable anterior and posterior termini forms and at least some limb buds are present, but segments are irregular or fail to form in the posterior terminus (Fig. 3D and E; ref. Fig. 7C of Setton and Sharma 2018); in this phenotypic class, the germband does not delaminate from the yolk (as with wild type embryogenesis). Class II phenotype embryos (n = 100/316) also bear recognizable anterior and posterior termini, but Class II embryos do not exhibit any appendage development, lack well-defined segments, and also do not delaminate from the yolk (Fig. 3F and G; ref. Fig. 7D of Setton and Sharma 2018). Class III phenotypes (n = 46/316) are comprised of a germband where at least one terminus of the AP axis cannot be reliably identified; segmental defects consist of truncated body regions (Fig. 3H) and/or failure to form segments (Fig. 3I); at least one section of tissue has delaminated from the yolk; and the germband is typically discontinuous (Fig. 3H–J; ref. Fig. 7F of Setton and Sharma 2018). Class IV phenotypes (n = 101/316) are comprised of a single disc of tissue that is circular, teardrop-shaped, or irregular, with no recognizable morphological landmarks (Fig. 3K; Figs. 7G, 8 L and 8 M of Setton and Sharma 2018); class IV phenotypes do not delaminate from the yolk. All four phenotypic classes consistently exhibited developmental arrest and never underwent deposition of cuticle (Supplementary Video S1). All observations spanned a minimum of three to a maximum of 21 days (wild type *P. tepidariorum* typically hatch in 186 h in laboratory conditions; Mittmann and Wolff 2012).

Supplementary data related to this article (including timelapse video) can be found at https://doi.org/10.1016/j.ydbio.2021.02.006.

A qPCR approach was used to validate our identification of *Ptep-arr*

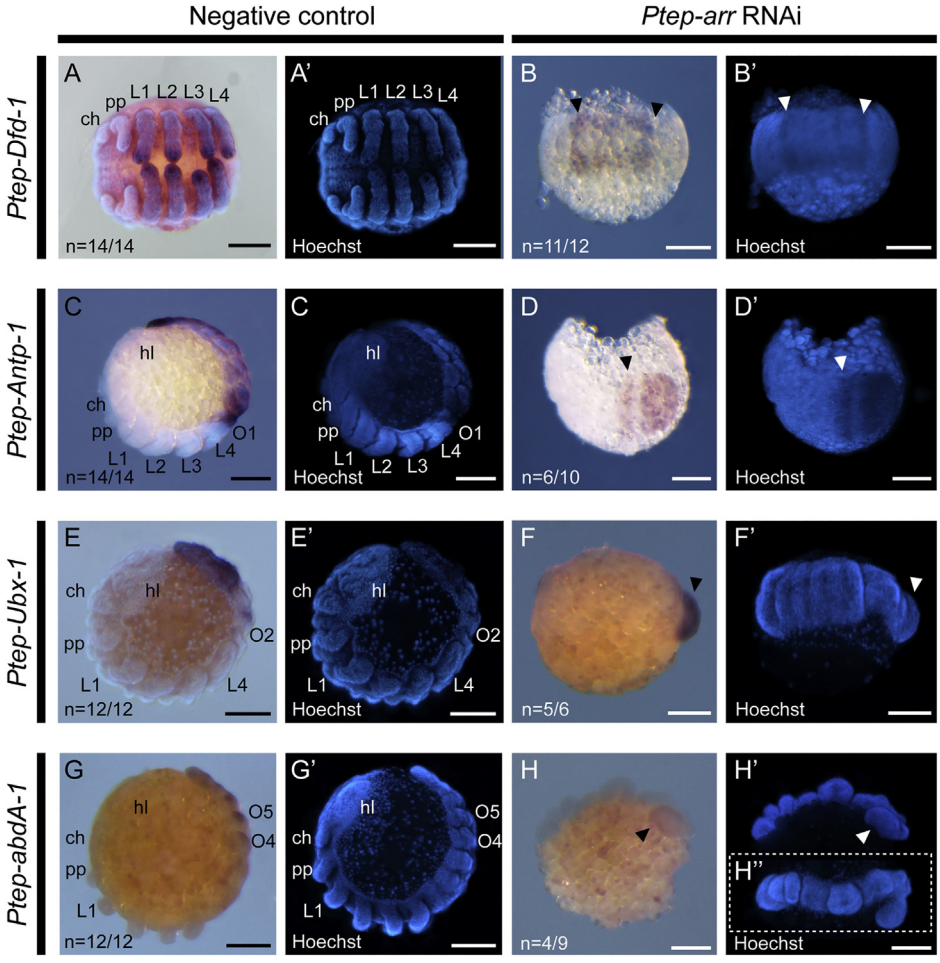

Fig. 4. Posterior Hox gene expression at 144 hAEL. (A) Expression of *Ptep-Dfd-1* in a negative control embryo showing expression restricted to L1-L4. (B) *Ptep-arr* RNAi embryos express *Ptep-Dfd-1* in a medial region of the AP axis (arrowheads) despite absence of segments and appendages. (C) Expression of *Ptep-Antp-1* in a negative control embryo is restricted to the opisthosoma (posterior tagma), which results from sequential addition of segments from the posterior growth zone. (D) *Ptep-arr* RNAi embryos express *Ptep-Antp-1* in a large domain at the posterior terminus of the germband. Arrowhead denotes anterior boundary of expression. (E) Expression of *Ptep-Ubx*-1 in a negative control embryo showing expression from O2 segment to posterior terminus. (F) Class II *Ptep-arr* RNAi embryo exhibiting *Ptep-Ubx-1* at the posterior terminus of the germband (arrowheads). Note the absence of limb buds and wild type head lobes. (G) Expression of *Ptep-abdA*-1 in a negative control embryo showing expression in posterior-most opisthosomal segments. (H) Class II *Ptep-arr* RNAi embryo exhibiting weak *Ptep-abdA-1* expression in the putative posterior terminus. (A′-H′) Counterstaining of images (A–H) using Hoechst. (H″) Dorsal view of same embryo in (H′). Abbreviations: O1, first opisthosomal segment. All other abbreviations as in Fig. 3. Anterior is to the left in all panels. (A, B) in ventral view; (C, D) in lateral or ventrolateral view. Scale bars: 100 μm.

phenotypes and account for the possibility we were categorizing dead embryos as phenotypes (Fig. 3L). First, we compared pooled RNAi embryos spanning Class I through Class IV (with the majority in class III-IV). We performed the sampling of embryos when the oldest embryos exhibiting wild type developmental from the same RNAi-treated clutch reached stage 14 (ventral closure stage; but compare to embryos in Fig. 3A and B). *Ptep-arr* LOF phenotype embryos exhibited decreased expression of *arr* relative to wild type counterparts (18.7–22.4%, average 20.5%).

To accommodate the possibility that Class III-IV phenotypes corresponded to younger developmental stages (note that the RNAi embryo shown in Fig. 3B resembles germband elongation stage embryos), we compared *Ptep-arr* expression of RNAi embryos to wild type embryos of stage 6 (dorsal field stage), stage 7 (germband stage), and stage 8.1 (prosomal limb bud stage) embryos. *Ptep-arr* was significantly less expressed in RNAi embryos than any group of negative control embryos (versus stage 6: 15.8–18.4%; versus stage 7: 21.3–23.9%; versus stage 8.1: 18.5–20.6%) (Fig. 3L). These results support the inference that the morphology of *Ptep-arr* RNAi embryos is linked to the knockdown of *Ptep-arr* expression levels.

To establish the cellular basis for the abnormal development of *Ptep-arr* RNAi embryos, we examined cell proliferation and cell death using fluorescent immunohistochemistry. With respect to negative control embryos, *Ptep-arr* RNAi embryos exhibit reduced cell proliferation by 120 hAEL (Fig. S4; $n = 8$ of 8). We did not detect differences in apoptosis at 120 hAEL between wild type and *Ptep-arr* RNAi embryos (Fig. S5; $n = 6$ of 6). These patterns of cellular process parallel the outcome of *wg* knockdown in the growth zone of the cockroach *P. americana* (Chesebro et al., 2013) and are consistent with disruption of cWnt signaling.

3.3. Posterior Hox gene expression in Ptep-arr RNAi embryos

To assess the completeness of the AP axis in the *Ptep-arr* LOF phenotype, we surveyed the expression of four Hox genes using whole mount *in situ* hybridization: *Deformed-1* (*Dfd-1*), a marker for the four leg-bearing segments of the prosoma; *Antennapedia-1* (*Antp-1*), a marker for the opisthosoma (the posterior, appendage-less tagma); *Ultrabithorax-1* (*Ubx-1*), a marker for opisthosomal segments O2 to the posterior terminus; and *abdominalA-1* (*abdA-1*), a marker for opisthosomal segments O3 to the posterior terminus. These markers were additionally selected for well-documented temporal expression (Schwager et al., 2017).

In *Ptep-arr* knockdown embryos, *Ptep-Dfd-1* was detected in a medial region of the germband that did not extend to the posterior terminus of the germband at 144 hAEL (Fig. 4A and B; $n = 18$ of 19). The strength of *Ptep-Dfd-1* expression was visibly diminished in the phenotypes by comparison to wild type counterparts, though this may reflect the smaller size and thickness of the *arr* RNAi germ bands rather than reduced expression strength. The opisthosomal marker *Ptep-Antp-1* was expressed at one terminus of the germband that we interpret to correspond to the presumptive opisthosomal territory (Fig. 4C and D; $n = 14$ of 19). Like *Ptep-Dfd-1*, expression of *Ptep-Antp-1* was also weaker in the RNAi phenotype when compared to wild type counterparts (Fig. 4D).

Ptep-Ubx-1 is expressed at stage 8 (prosomal limb bud stage) in wild type spider embryogenesis and its anterior boundary demarcates the second opisthosomal (O2) segment (Fig. 4E; Schwager et al., 2017). In *Ptep-arr* knockdown embryos, we detected expression of *Ptep-Ubx-1* in the putative posterior terminus in class II and class III embryos (Fig. 4F; $n = 5$ of 6). Wild type *Ptep-abdA-1* expression commences at stage 9 (limb differentiation stage) and spans the O3 segment to the posterior terminus (Fig. 4G; Schwager et al., 2017). In *Ptep-arr* knockdown embryos, weak expression of *Ptep-abdA-1* was detected at one pole of class II and class III embryos ($n = 4$ of 9; Fig. 4H).

These assays suggest that *Ptep-arr* RNAi embryos retain posterior axis identity despite disruption of segmentation.

3.4. Differential gene expression (DGE) analysis of spider RNAi experiments

Whereas the hemimetabolous insect RNAi phenotype accorded closely with previously described posterior axis defects in *T. castaneum*, the spider *arr* LOF phenotype differed in its broader range of AP axis defects, as well as developmental arrest prior to cuticle deposition. The retention of posterior Hox expression in spider *arr* LOF phenotypes was also unexpected (Fig. 4). To characterize comprehensively the systemic effects of cWnt disruption in the spider, we generated RNA-seq data for *Ptep-arr* knockdown and negative control experiments at 120 and 144 hAEL (Fig. S6A; Tables S2, S4), leveraging the availability of the reference genome of *P. tepidariorum* for read quantification (Schwager et al., 2017). Our sampling of *Ptep-arr* phenotypes spanned all observable phenotypes (majority Class III and Class IV) at two time points. Analysis of comparative gene expression showed that biological replicates clustered together as a function of experimental treatment under both principal components analyses (PCA) and assumption-free hierarchical clustering on expression data (Fig. 5A, Fig. 5B, S6B, S6C). We first surveyed the target gene *Ptep-arr* for changes in expression in our DGE dataset. Differential expression analyses indicated that *Ptep-arr* was down-regulated by 50.5% (range: 35.2–62.2%) at 120 hAEL compared to negative controls. DGE analysis at 144 hAEL also recovered *Ptep-arr* as lowly expressed, but without significance (Fig. 5G). Notably, the selection of a broad range of phenotypes for RNA-Seq exhibited less significant knockdown of *Ptep-arr* compared to quantitation using qPCR (compare Figs. 5G to 3L), which may be attributable to (1) the inclusion of less severe phenotypes in the RNA sequencing and (2) the use of a smaller dsRNA fragment (albeit same concentration by mass) for knockdown in qPCR assays. Comparison of read mapping density for the *arr* locus across experiments confirmed lower quantity of reads mapped in RNAi treatments, as well as similar density distributions both within and outside the bounds of the amplicon designed for RNAi (Fig. S7).

DGE analysis revealed numerous differentially expressed genes between experiments; we contextually defined significant hits as $p_{adj} \leq 0.05$ and $\log_2$-fold change ≥ 2. At 144 hAEL, DGE analyses revealed a much larger number of significantly affected candidates ($n = 1183$) than at 120 hAEL ($n = 272$; Fig. 5B), which may reflect indirect downstream effects stemming from the absence of entire morphological structures or organs in *Ptep-arr* RNAi embryos (Fig. 5B, D). To facilitate clustering analysis, we examined genes exhibiting $\log_2$-fold change ≥ 3 for 144 hAEL, reducing the number of significantly affected candidates ($n = 448$). Cutting the hierarchical clustering tree at 50% height for both datasets resulted in two clusters (Fig. 5A and B), which corresponded to overall expression patterns showing up- or down-regulation of genes in *Ptep-arr* RNAi embryos, relative to negative controls. At 120 hAEL, the 50 most significantly lowly expressed genes (by adjusted p-value, p_{adj}) in the knockdown experiments included homologs of vertebrate or *D. melanogaster* genes involved in organogenesis, neurogenesis, and germline development (Table S5). At this same time point, the 50 most significantly overexpressed genes in the *Ptep-arr*-RNAi embryos were comprised of ribosomal proteins, nucleolar proteins, kinases, tyrosine-kinases, members of the myc/TOR pathways, and numerous uncharacterized genes (e.g., orphan genes; Table S5). Summary statistics for queried genes are provided in Table S6.

3.5. RNAi against Ptep-arr: Wnt signaling and segment polarity genes

We next surveyed specific pathways and homologs involved in axis patterning, prioritizing Wnt signaling. Six of the seven canonical Wnt homologs of *P. tepidariorum* (*Ptep-wg/Wnt1, Ptep-Wnt2, Ptep-Wnt6*, *Ptep-Wnt7-1, Ptep-Wnt7-2*, and *Ptep-Wnt16*) were down-regulated and four of these significantly so ($p_{adj} < 0.05$) for at least one time point (Fig. 5E). These data are consistent with our previous report of loss of *Ptep-wg* expression in in *Ptep-arr* RNAi embryos, using *in situ* hybridization (Setton and Sharma 2018). The non-canonical Wnts *Ptep-Wnt4*, *Ptep-Wnt5*,

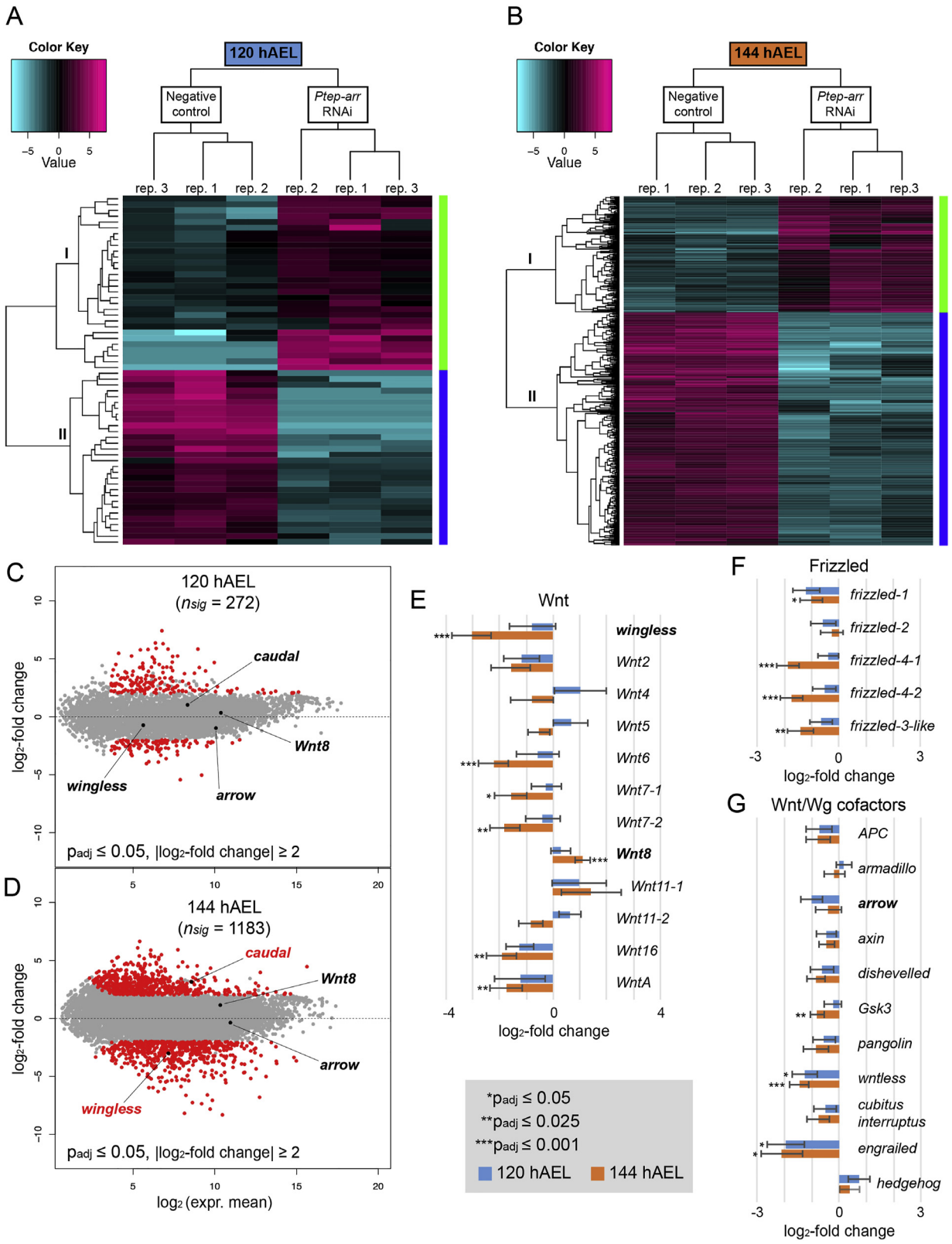

Fig. 5. Systemic effects of *Ptep-arr* knockdown during spider embryogenesis. (A) Heatmap of hierarchically clustered differentially expressed ($p_{adj} \leq 0.05$, log_2-fold change ≥ 2) genes at 120 hAEL. Genes are displayed as rows, samples as columns. Overexpression is colored pink, underexpression blue. Roman numerals indicate clusters generated by cutting the hierarchical clustering tree (left) at 50% of tree height. (B) Heatmap of hierarchically clustered differentially expressed ($p_{adj} \leq 0.05$, log_2-fold change ≥ 3) genes at 144 hAEL. (C–D) MA plots showing differentially expressed genes at 120 hAEL ($p_{adj} \leq 0.05$, log_2-fold change ≥ 2) (C) and 144 hAEL ($p_{adj} \leq 0.05$, log_2-fold change ≥ 3) (D). Significantly differentially expressed genes in red. (E–G) Effects of *Ptep-arr* RNAi on selected signaling pathways. (E) Wnt gene family, (F) Frizzled gene family, (G) co-receptors and cofactors of Wnt signaling. Asterisks and colors in (E–G) indicate significance and time of sampling, following inset legend.

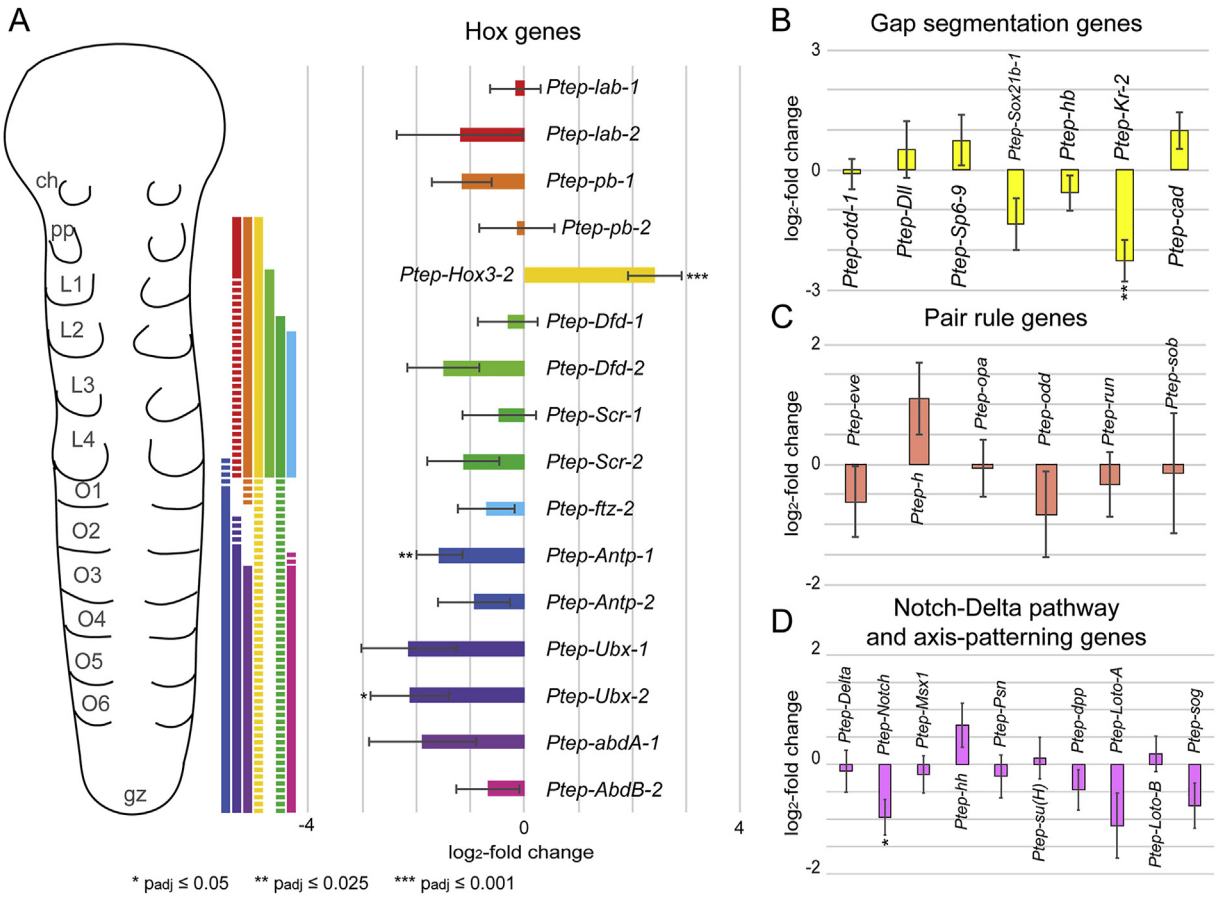

Fig. 6. Effects of *Ptep-arr* RNAi on the AP axis and the segmentation cascade. (A) Schematic of wild type expression domains of Hox genes in *P. tepidariorum* (following Schwager et al., 2017) and differential expression of Hox genes at 120 hAEL in *Ptep-arr* RNAi embryos. (B) Differential expression of gap segmentation genes in *Ptep-arr* RNAi embryos at 120 hAEL. (C) Differential expression of homologs of pair rule genes with known expression patterns in the spider at 120 hAEL. (D) Differential expression of Notch-Delta pathway and selected axis-patterning genes with known functions in *Ptep-arr* RNAi embryos at 120 hAEL.

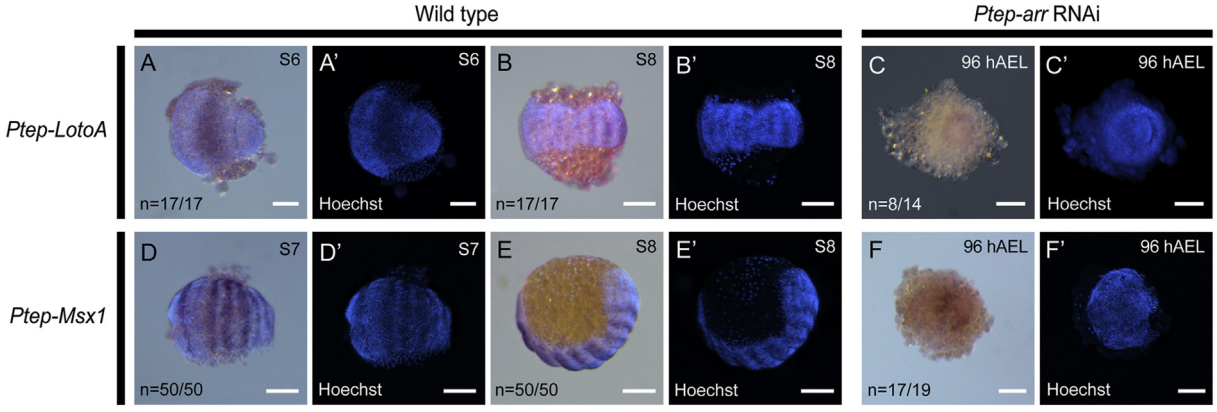

Fig. 7. Knockdown of *Ptep-arr* disrupts Toll and Hh signaling. (A, B) Wild type expression of *Ptep-LotoA* at stage 6 (A) and stage 8 (B). (C) *Ptep-arr* RNAi embryos exhibit faint and disrupted expression of *Ptep-LotoA*. (D, E) Wild type expression of *Ptep-Msx1* at stage 7 (D) and stage 8 (E). (F) *Ptep-arr* RNAi embryos exhibit faint and disrupted expression of *Ptep-Msx1*. Scale bars: 100 μm.

and *Ptep-Wnt11-2* exhibited non-significant variation across sampled time points, whereas *Ptep-Wnt11-1* was non-significantly overexpressed at both time points. Oddly, expression of *Ptep-Wnt8*, a canonical Wnt homolog, was either unaffected (at 120 hAEL; $\log_2$-fold change = 0.300, p_{adj} = 0.6026) or significantly higher than negative control levels (144 hAEL; $\log_2$-fold change = 1.103, p_{adj} = 0.0007) in the *Ptep-arr* RNAi embryos. We investigated this anomalous result in detail, in conjunction with its target *Ptep-cad* (see below).

We next investigated how *Ptep-arr* RNAi affected expression of *frizzled* homologs (Fig. 5F). In addition to the four *P. tepidariorum fz* homologs previously isolated by Sanger sequencing, we discovered a new *fz* homolog in the *P. tepidariorum* genome (XM016069089.2) that formed a grade with *fz3* orthologs of Onychophora and Mandibulata (Fig. S8). Expression of all *fz* homologs was reduced at both sampled time points, and significantly so at 144 hAEL for the *fz1* ortholog (p_{adj} = 0.0492), the two *fz4* paralogs (*fz4-1*: p_{adj} = 0.0001; *fz4-2*: p_{adj} = 0.0003) and the

putative *fz3* ortholog ($p_{adj} = 0.016$).

Examination of other members of the Wnt signaling pathway (Fig. 5G; Fig. S9) revealed reduced expression of the Wnt partner *wntless* ($p_{adj} = 0.0467$ at 120 hAEL; $p_{adj} = 0.0003$ at 144 hAEL). *pangolin* and *axin* were mildly downregulated, without significance (log_2-fold change ≥ -1). *β-catenin* (*armadillo*) expression was unaffected by *Ptep-arr* RNAi (Table S5). Consistent with a segmentation phenotype with disruption of *wg*, expression was reduced for segment polarity genes, such as *Ptep-en-1*, which is not detected in *Ptep-arr* RNAi embryos using *in situ* hybridization at 120 or 144 hAEL (Setton and Sharma 2018), and is congruently recovered as downregulated in *Ptep-arr* RNAi embryos at this significance level for both time points (log_2-fold change $= -1.95$ and $p_{adj} = 0.037$ at 120 hAEL; log_2-fold change $= -2.11$ and $p_{adj} = 0.026$ at 144 hAEL). At both sampled time points, *Ptep-cubitus interruptus* was mildly downregulated, and *Ptep-hedgehog* exhibited mild overexpression (Fig. 5G).

These results are broadly consistent with a conserved role for *Ptep-arr* in cWnt signaling and segmentation in the spider.

3.6. RNAi against Ptep-arr: The higher segmentation cascade

To assess how higher levels of the segmentation pathway had been disrupted by *Ptep-arr* knockdown, we examined a suite of genes whose expression and/or functional data substantiate their involvement in AP segmentation.

Nineteen Hox genes occur in the *P. tepidariorum* genome (Schwager et al., 2017); of these, 16 were recovered in DGE analysis at 120 hAEL (Fig. 6*A*). Significant differential expression was observed only for *Ptep-Hox3-2* (log_2-fold change $= 2.410$; $p_{adj} = 0.0002$), *Ptep-Antp-1* (log_2-fold change $= -1.586$; $p_{adj} = 0.0060$), and *Ptep-Ubx-2* (log_2-fold change $= -2.134$; $p_{adj} = 0.0327$). Some expression was retained for at least one paralog of each Hox gene; together with *in situ* hybridization assays (Fig. 4), these patterns corroborate the inference that the *Ptep-arr* RNAi phenotype does not represent a truncation of the AP axis.

We therefore surveyed known gap segmentation genes in the spider, as well as homologs of classical gap genes identified in *Drosophila melanogaster*, for changes in transcription levels at 120 hAEL. Only the earlier time point (120 hAEL) was investigated here, as segmentation is completed before 144 hAEL in wild type embryogenesis and many gap genes exhibit pleiotropy of function (Mittmann and Wolff 2012; Setton and Sharma 2018). In *P. tepidariorum*, genes that exhibit demonstrable gap gene function consist of *orthodenticle-1* (*otd-1*; Pechmann et al., 2009), *hunchback* (*hb*; Schwager et al., 2009), *Sp6-9* (Setton and Sharma 2018), *Distal-less* (*Dll*; Pechmann et al., 2011), and *Sox-21b-1* (Paese et al., 2018). DGE analyses showed that expression of *Ptep-otd-1*, *Ptep-Dll* and *Ptep-Sp6-9* was not affected (Fig. 6B), consistent with *in situ* hybridization data showing retention of *Ptep-otd-1* and *Ptep-Sp6-9* in *Ptep-arr*-RNAi embryos (Setton and Sharma 2018). Changes in expression were not significant for *Ptep-hb* or *Ptep-Sox21b-1*, though the latter did exhibit mild downregulation (log_2-fold change $= -1.352$). One exception to this trend was the significant downregulation of *Ptep-Kr-2* at 120 hAEL (log_2-fold change $= -2.282$, $p_{adj} = 0.0012$) (Fig. 6B).

No functional data are available for homologs of pair rule genes in spiders (Damen 2007). We surveyed *P. tepidariorum* homologs of classical pair rule genes, emphasizing candidates whose expression patterns in spiders have suggested involvement in opisthosomal segmentation (e.g., *hairy*, *even-skipped*, *runt*; Damen et al., 2000) and whose homologs have been functionally linked to posterior segmentation in short germ insects (Mito et al., 2007; Choe and Brown 2009; Auman and Chipman 2018). DGE analyses suggested that none of these genes were significantly affected by *Ptep-arr* RNAi at 120 hAEL (Fig. 6C).

We then surveyed members of the Notch-Delta pathway, which has been established as a mechanism underlying posterior segment addition in spiders; Notch-Delta signaling plays a key role in establishing the caudal lobe that will generate opisthosomal segments, with RNAi against *Delta* (*Dl*), *Notch* (*N*) or *Suppressor of Hairless* (*Su(H)*) incurring depletion of *cad* and an array of segmental defects (Stollewerk et al., 2003; Schoppmeier and Damen 2005; Oda et al., 2007). *Ptep-Notch* (*N*) was significantly down-regulated at 120 hAEL in *Ptep-arr* RNAi embryos (log_2-fold change $= -0.966$, $p_{adj} = 0.0312$), whereas *Ptep-Delta* (*Dl*) was not affected (Fig. 6D). *Su(H)* and *presenilin*, two members of the Notch-Delta pathway with established segmentation phenotypes in spiders, were unaffected at 120 hAEL (Schoppmeier and Damen 2005) (Fig. 6D). Axis specification and axis elongation genes with established functions (*decapentaplegic*, *short gastrulation*, *smoothened*, *Long Toll A* [*LotoA*], and *Long Toll B* [*LotoB*] (Akiyama-Oda, 2006; Benton et al., 2016) were also not significantly affected, though *LotoA* exhibited mild downregulation (log_2-fold change $= -1.115$). Lastly, while expression of *hedgehog* was mildly affected in *Ptep-arr* RNAi embryos (log_2-fold change $= 0.720$, $p_{adj} = 0.2059$), expression of its downstream target *Msx1* was not substantially altered (log_2-fold change $= -0.180$).

Taken together, these results suggest that knockdown of *Ptep-arr* has systemic effects across posterior segmentation and elongation developmental processes in the spider.

3.7. RNAi against Ptep-arr disrupts Toll and Hedgehog signaling

Mild downregulation of gene expression inferred by the DGE approach is difficult to interpret, as modest reduction of transcript quantity is not synonymous with retention of spatial organization. To validate the bioinformatic predictions of the DGE approach on two major signaling pathways, we additionally surveyed the expression of two spider-specific paralogs using *in situ* hybridization (Fig. 7). *LotoA* is a member of the Toll pathway and is required for posterior axis elongation (Benton et al., 2016). Weak expression of *LotoA* was detected in severe *Ptep-arr* LOF phenotypes (Fig. 7C), although the spatially disrupted expression pattern did not correspond to wild type expression at any stage of spider development. *Msx1* is a member of the Hedgehog signaling pathway and has recently been shown to play a key role in both prosomal and opisthosomal segmentation of *P. tepidariorum* (Akiyama-Oda and Oda 2020). As with *Ptep-LotoA*, we detected expression of *Ptep-Msx1*, but the expression pattern did not correspond to repeating stripes, as observed in wild type embryogenesis (Fig. 7F).

These results are consistent with the predictions of the DGE analysis (i.e., mild knockdown), but suggest that knockdown of *Ptep-arr* can have greater effects on signaling pathways than predicted by bioinformatic investigations alone. In addition, these results are consistent with the small size of *Ptep-arr* embryos (due to disruption of Toll signaling) and the lack of segments throughout the germband (due to disruption of Hh signaling).

3.8. RNAi against arr homologs does not abrogate Wnt8 expression in Arthropoda

Of the canonical Wnt homologs, functional data in *P. tepidariorum* are only available for *Ptep-Wnt8*, which has been shown to be required for the establishment of the posterior growth zone and the opisthosomal segments (Mcgregor et al., 2008). Contrary to the response of other canonical Wnts, *Ptep-Wnt8* was overexpressed at both sampled time points in *Ptep-arr* RNAi embryos, with significant up-regulation at 144 hAEL (Fig. 5E). *Ptep-Wnt8* has been shown to act upstream of *Ptep-cad* to establish the posterior growth zone and may also play a role in delimiting *Ptep-Krüppel-2* (*Kr-2*) expression in the L3/L4 segments; knockdown of *Ptep-Wnt8* results in loss of *Ptep-cad* expression and expansion of the L3/L4 expression domain of *Ptep-Kr-2* (Mcgregor et al., 2008). We therefore investigated whether *Ptep-cad* and *Ptep-Kr-2* were also affected by *Ptep-arr* RNAi. DGE analyses showed that *Ptep-cad* was non-significantly up-regulated in *Ptep-arr* RNAi embryos at 120 hAEL (log_2-fold change $= 0.989$, $p_{adj} = 0.1167$), and significantly so at 144 hAEL ($p_{adj} = 3.142$; $p_{adj} = 8.7 \times 10^{-7}$) (Fig. 5). Intriguingly, *Ptep-Kr-2* was significantly down-regulated in the knockdown at 120 hAEL (Fig. 6B), consistent with reduction of the L3/L4 territory (the inverse effect of *Ptep-Wnt8* depletion; Mcgregor et al., 2008).

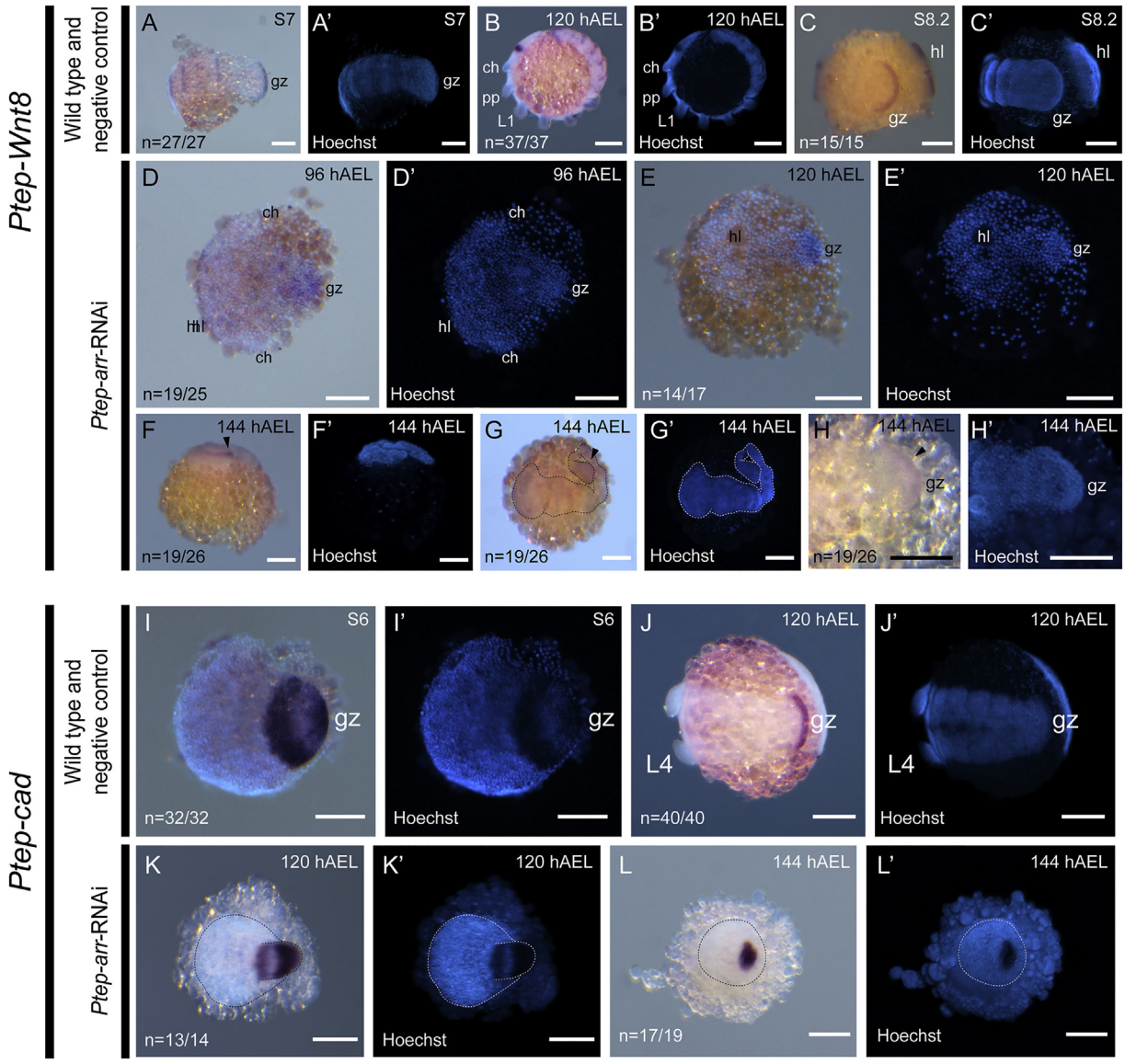

Fig. 8. *Ptep-arr* RNAi retain expression of *Ptep-Wnt8* and *Ptep-cad*. (A–C) Wild type expression of *Ptep-Wnt8* at stage 7 (A) and negative control embryos at 120 hAEL (B, C). Note stripes of expression in prosomal segments, in addition to a strong expression domain in the posterior growth zone (C). (D–F) In *Ptep-arr* RNAi embryos, weak expression of *Ptep-Wnt8* is detected at 144 hAEL, particularly in the growth zone (E, F). (G, H). Expression of *Ptep-cad* in wild type stage 7 (G) and negative control embryos (H). (I, J) *Ptep-arr* RNAi embryos exhibit comparable expression of *Ptep-cad* with respect to expression strength in the posterior terminus and possible spatial expansion into the anterior of the germband in Class IV embryos. Abbreviations: gz: posterior growth zone. All other abbreviations as in Fig. 3. (A′-J) Counterstaining of images (A–J) using Hoechst. Scale bars: 100 μm.

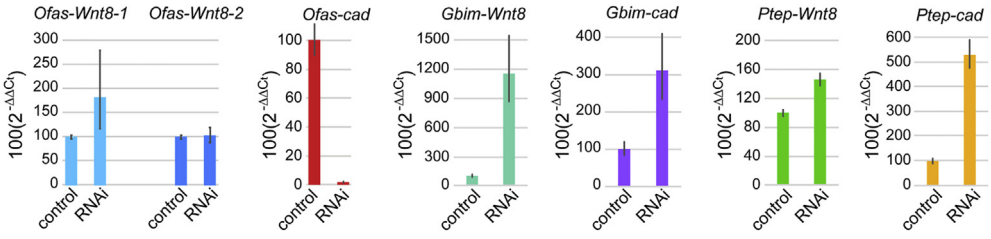

Fig. 9. Quantitation of *Wnt8* and *cad* homologs upon knockdown of *arr* in *O. fasciatus*, *G. bimaculatus*, and *P. tepidariorum*. In all target species, expression of *Wnt8* is unaffected (*Ofas-Wnt8-2*) or increased (remaining homologs) by knockdown of *arr*. Expression of *cad* is greatly diminished in *Ofas-arr* RNAi embryos; unaffected in *Gbim-arr* RNAi embryos; and increased in *Ptep-arr* RNAi embryos (relative to negative control embryos of the same age).

To validate these inferences based on DGE analysis, we assayed the spatial expression of *Ptep-Wnt8* and *Ptep-cad* using *in situ* hybridization in *Ptep-arr* RNAi embryos (Fig. 8). In wild type spider germ bands, *Ptep-Wnt8* is expressed as stripes corresponding to the posterior compartment of each segment, in addition to a broad domain in the posterior growth zone (Fig. 8A–C), whereas *Ptep-cad* is restricted to the posterior growth

zone (Fig. 8I and J) (Mcgregor et al., 2008). *In situ* hybridization revealed that *Ptep-arr* RNAi embryos do not undergo loss of *Ptep-Wnt8* expression in the posterior growth zone from 96 to 144 hAEL (Fig. 8D–H; $n = 52$ of 68). Between 72 and 96 hAEL, assayed RNAi embryos exhibited morphology and *Wnt8* expression similar to wild type counterparts (Supplementary Video S1); we therefore cannot rule out that embryos assayed in those earlier time points represent wild type embryogenesis, rather than *Ptep-arr* loss-of-function phenotypes.

In *Ptep-arr* RNAi embryos, *Ptep-cad* expression was retained even in the most severe phenotypes (Fig. 8K, L). As with *Wnt8*, *Ptep-arr* RNAi embryos assayed between 72 and 96 hAEL exhibited morphology and *cad* expression comparable to wild type embryos (not shown), which precludes us from ruling out incomplete penetrance of RNAi. qPCR assays for *Ptep-Wnt8* and *Ptep-cad* substantiated inferences based on DGE analyses and *in situ* hybridization, showing increased expression of these genes in *Ptep-arr* RNAi embryos (Fig. 9). *Ptep-arr* RNAi phenotypes exhibited 37.6–54.0% (average 45.6%) greater *Wnt8* expression, and over four-fold greater *cad* expression, than wild type embryos of the same age.

To assess whether the independence of *Wnt8* expression from cWnt signaling is systemic across arthropods, we performed qPCR for all *Wnt8* homologs, as well as its target *cad*, in the two hemimetabolous insects. In *O. fasciatus*, knockdown of *Ofas-arr* resulted in overexpression of *Ofas-Wnt8-1* and no change in expression of *Ofas-Wnt8-2* (Fig. 8). However, *Ofas-cad* expression was greatly diminished in *Ofas-arr* RNAi embryos. In the cricket *G. bimaculatus*, higher expression of both *Wnt8* and *cad* was observed, relative to negative control experiments (Fig. 9).

In summary, our data suggest that knockdown of arthropod *arr* homologs does not result in the loss of *Wnt8* expression, as previously shown in *T. castaneum* (Bolognesi et al., 2009).

4. Discussion

A role for Wnt-Cad signaling in posterior segment addition is held to be an ancestral feature of Arthropoda, and possibly distantly related segmented phyla (Copf et al., 2004; Bolognesi et al., 2008a; Mcgregor et al., 2008; Martin and Kimelman 2009; Mcgregor et al., 2009 but see Fritzenwanker et al., 2019). Within the arthropods, the acceptance of an evolutionarily conserved role for Wnt signaling in segmentation is based largely upon phenetic analyses of gene expression patterns for segmentation gene homologs (e.g., Dearden and Akam 2001; Damen 2002; Hughes and Kaufman 2002; O'Donnell and Jockusch 2010). Yet, this abundance of conserved expression patterns belies a dearth of experimental evidence supporting evolutionary conservation of gene regulatory networks over large phylogenetic distances. Only two datasets addressing *Wnt8* function in the beetle *T. castaneum* and the spider *P. tepidariorum* have demonstrated conserved function of a Wnt ortholog in the lineages whose divergence represents the common ancestor of all arthropods (Mcgregor et al., 2008; Bolognesi et al., 2008a). Other Wnt homologs lack functional data in short germ arthropods altogether or have proven remarkably recalcitrant to knockdown (e.g., Miyawaki et al., 2004). This phenomenon may be partially attributable to functional redundancy of the Wnts in short germ arthropods, though data supporting this postulate are similarly limited (Bolognesi et al. 2008a, 2008b). Furthermore, datasets assessing the downstream targets of Wnt homologs are often incongruous upon comparison. As an example, comparable posterior truncation phenotypes have been observed upon knockdown of either Wnt homologs or *cad* in other short germ arthropods (Copf et al., 2004; Shinmyo et al., 2005; Bolognesi et al., 2008a; Chesebro et al., 2013), but the effect of Wnt inhibition on *cad* expression been assessed directly only in the cockroach *P. americana* (for *wg*; Chesebro et al., 2013) and in the spider *P. tepidariorum* (for *Wnt8*; Mcgregor et al., 2008).

To circumvent these limitations, we systemically inhibited cWnt signaling in non-model arthropods by targeting the Wnt co-receptor *arr*. Within arthropods, *arr* LOF phenotypes have only been described in two insect species, but those phenotypes differ from each other and from the phenotype we obtained in the spider *P. tepidariorum*. In the fruit fly *D. melanogaster*, *arr* LOF mutants (i.e., lacking both maternal and zygotic *arr* function) exhibit a segment polarity phenotype that is indistinguishable from a *wg* LOF phenotype, albeit with proper distribution of Wg protein (Wehrli et al., 2000). In the short germ insect *T. castaneum*, RNAi against *Tcas-arr* disrupts posterior segmentation, resulting in embryos with small, rudimentary heads (with cuticle), no trunk region, reduction in Engrailed expression stripes, and disruption or loss of *wg* expression during early germband elongation and germband extension stages (Bolognesi et al., 2009). Severe *arr* RNAi phenotypes in *T. castaneum* exhibited complete loss of segments and appendages, and retained no morphological landmarks other than part of the foregut, but these embryos still underwent deposition of cuticle (Beermann et al., 2011).

Our results, together with the *T. castaneum* dataset, suggest that *arr* (and by extension cWnt signaling) plays a conserved role in posterior axis patterning across Arthropoda. The posterior truncation phenotypes we observed within subsets of the phenotypic spectra of all three species are comparable to their *T. castaneum* counterpart (Bolognesi et al., 2009). Within the hemimetabolous insects, the extent of the affected region accords directly with the mode of segmentation (defects posterior to the anterior head in the short germ *O. fasciatus*, and posterior to the T2 leg in the intermediate germ *G. bimaculatus*). However, due to the differing degree of knockdown efficiency between the two species, we cannot rule out that a more efficient knockdown in the cricket could affect more anterior segments.

The *P. tepidariorum arr* RNAi phenotypic spectrum was more variable and challenging to interpret than its insect counterparts, in that the germ band did not always exhibit posterior truncation of the AP axis. Expression assays of anterior (Setton and Sharma 2018), trunk (i.e., posterior prosomal) and posterior (opisthosomal) Hox genes support the inference that the germ band is regionalized in some *Ptep-arr* RNAi embryos and that the posterior Hox-positive territory formed by posterior segment addition during wild type embryogenesis is correctly specified. Such embryos were previously shown to be deficient for *wg* and *en-1* expression using *in situ* hybridization (Setton and Sharma 2018). One possible interpretation of these embryos was that they could represent wild type phenotypes incurred by developmental delay. However, the timing of onset for the posterior Hox genes *Ultrabithorax-1* and *abdominal-A-1* (stages 8.2 and 9.1, respectively; Schwager et al., 2017) is associated with clearly recognizable morphological landmarks in wild type development, including all prosomal appendages and segments (Mittmann and Wolff 2012), which were not observed in these RNAi embryos. Furthermore, qPCR analysis of *arr* expression against an array of wild type stages (stages 6–8, 14) refutes the interpretation that this phenotype can be classified as wild type embryos incurring RNAi-induced developmental delays.

In the weakest of the *Ptep-arr* RNAi phenotypes (Class I), we were able to observe some morphological landmarks, including the head lobes, stomadeum, and some appendages. These phenotypes exhibited clear deviations from wild type development, exhibiting defects of AP axis patterning that could affect anterior, median, or posterior territories; defects limited to the posterior growth zone; and/or defects affecting segmentation in a subset of somites. Moreover, a subset of the *P. tepidariorum* phenotypic spectrum, wherein segmentation defects were limited to the opisthosoma (e.g., Fig. 3E and I), links the effect of *arr* disruption to the phenotypic spectra of *O. fasciatus* and *G. bimaculatus* (compare to Figs. 1D and 2J).

The severe *Ptep-arr* loss-of-function phenotype represents a rare case of an arthropod Wnt segmentation phenotype outside of insects that affects the entire germband. To capitalize upon this window into the effects of systemic disruption of Wnt signaling in a phylogenetically significant lineage, we performed differential gene expression analysis through RNA-Seq datasets and leveraged the high-quality *P. tepidariorum* reference genome (Schwager et al., 2017), with the specific aim of characterizing the impact of *arr* knockdown on posterior axis patterning genes.

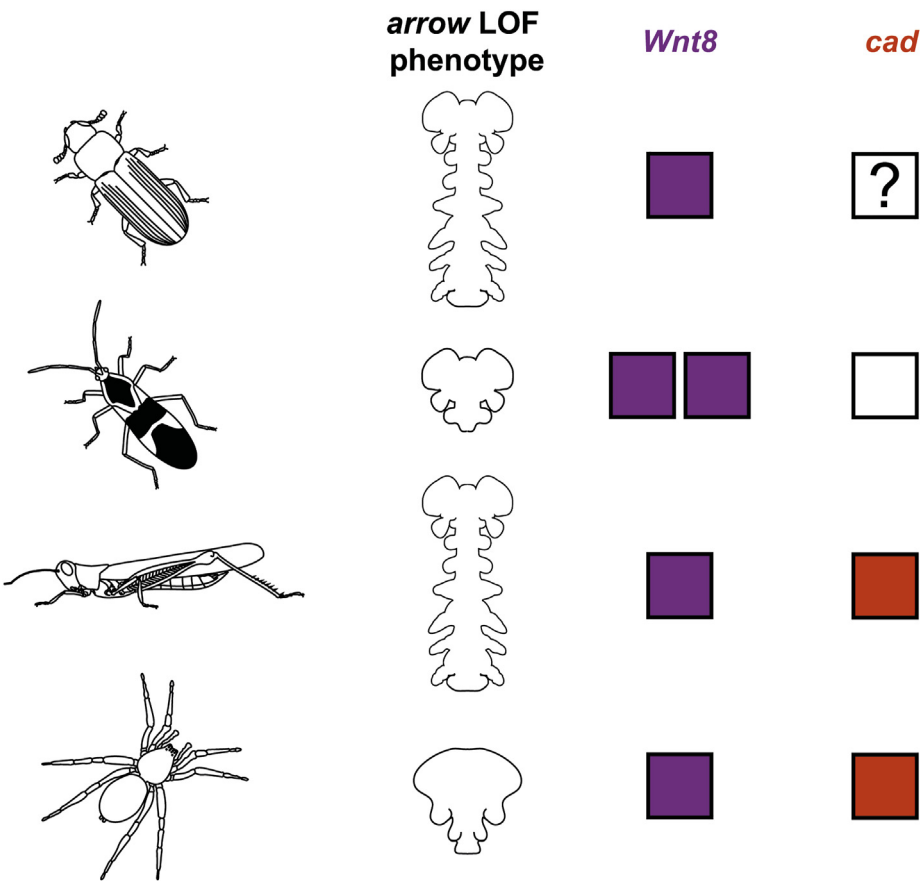

Fig. 10. Summary of functional data points for *arrow* homologs across short germ Arthropoda. From the top: *T. castaneum*, *O. fasciatus*, *G. bimaculatus*, and *P. tepidariorum*. Schematics indicate selected representations of the *arr* loss-of-function (LOF) phenotypic spectrum (from Fig. 2F of Bolognesi et al., 2009 for *T. castaneum*; remaining schematics from this study). Shaded boxes indicate retention of *Wnt8* (purple) or *cad* (red) in *arr* RNAi embryos of each species. Paired boxes for *O. fasciatus* indicate *Wnt8* duplicates.

DGE analyses revealed the surprising outcome that *Wnt8* and *cad* are unaffected by cWnt signaling in *Ptep-arr* RNAi embryos, a result substantiated by *in situ* hybridization. Using qPCR, we further demonstrated that all three *Wnt8* homologs of the hemimetabolous insects we surveyed were similarly affected by knockdown of *arr*. Intriguingly, this result parallels the retention of *Wnt8* upon knockdown of *arr* in the beetle *T. castaneum* at two sampled time points during germ band segmentation (Fig. 3 of Bolognesi et al., 2009). In wild type embryos of *T. castaneum*, *Wnt8* is expressed only in the posterior terminus, corresponding to the territory of spider *arr* RNAi germ bands where *Wnt8* expression is retained. Knockdown of *arr* in the beetle does not result in appreciable loss of *Wnt8* expression; only the fusion of the paired posterior expression domains of *Wnt8* distinguish *Tcas-arr* RNAi germ bands from wild type counterparts. The outcome that the posterior domain of *Ptep-Wnt8* is also unaffected by *arr* RNAi suggests that *Wnt8* may not be a target of cWnt signaling across Arthropoda generally. By contrast, measurable disruption of *wg* upon knockdown of *arr* appears to be conserved in *T. castaneum* and *P. tepidariorum* (Bolognesi et al., 2009; Setton and Sharma 2018).

A compelling difference between the *T. castaneum/O. fasciatus* phenotypic spectrum and those of *P. tepidariorum* and *G. bimaculatus* is the retention of *cad* in the spider and cricket RNAi embryos, as inferred by DGE analyses, qPCR, *in situ* hybridization, or some combination of these (Fig. 10). We add the caveat that the seeming overexpression of *cad* may result from severely misshapen embryos, which may lead to exaggerated relative expression. Nevertheless, this retention of *cad* may coincide with the severity of the posterior truncation phenotype; in both *P. tepidariorum* and *G. bimaculatus* phenotypes, some component of the posterior axis is retained, whereas the *T. castaneum/O. fasciatus* phenotype exhibits complete truncation of the germband posterior to the intercalary segment. In addition, *cad* expression in *Ptep-arr* RNAi embryos was correlated with retention of Hox, gap, and pair rule gene expression throughout the germ band; Cdx homologs of vertebrates positively regulate posterior Hox genes, and *cad* has been shown to positively regulate the pair rule gene *even-skipped* in both *T. castaneum* (Copf et al., 2004; Shinmyo et al., 2005; Chesebro et al., 2013; El-Sherif et al., 2014) and *P. tepidariorum* (Schönauer et al., 2016). Beyond Wnt-*cad* signaling, knockdown of *arr* also resulted in the depletion of *N*, which is consistent with the unsegmented *Ptep-arr* LOF phenotype and the regulatory model of spider posterior growth zone dynamics, wherein Notch-Delta signaling is postulated to repress *Wnt8*, which in turn promotes the expression of *cad* (Schönauer et al., 2016).

However, we add the caveat that the functions of many of the posterior Hox and segmentation gene homologs remain unknown in spiders. It has not been shown in short germ arthropods that *cad* regulates the posterior Hox genes, as has been demonstrated in vertebrate models (Ehrman and Yutzey 2001). Furthermore, a previous investigation of Frizzled function in *T. castaneum* showed that even embryos exhibiting severe collapse of the growth zone (incurred by knockdown of *frz1/2*) retain some *cad* expression (Fig. 4V–X of Beerman et al., 2011). As a result, we cannot rule out the possibility of conserved dynamics between cWnt and Cad signaling across the short germ arthropod species studied herein.

5. Conclusion

Our results demonstrate a conserved role for *arr* homologs (and by extension, cWnt signaling) in patterning the posterior axis across Arthropoda, with knockdown of *arr* demonstrably interfering with posterior segmentation in hemimetabolous insects and an arachnid (Fig. 10). RNA-Seq datasets generated herein provide for the first time a window into downstream effects of Wnt signaling inhibition in a non-insect arthropod. Our approach highlights the diagnostic power of differential gene expression tools in categorizing catastrophic phenotypes in non-model organisms.

Acknowledgements

We are indebted to Cassandra G. Extavour and Taro Nakamura for access to the *G. bimaculatus* system. Taro Nakamura shared a sequence of *Gbim-Wnt8* from an unpublished resource that aided qPCR primer design. Jesús Ballesteros provided bioinformatic assistance with R scripts. Rachel M. Smaby assisted with collection of *O. fasciatus* knockdown data. Comments from Jesús Ballesteros, Guilherme Gainett, Efrat Gavish-Regev, Carlos Santibáñez-López, and two anonymous reviewers improved a previous draft of this work. Sequencing was performed at the University of Wisconsin-Madison BioTechnology Center. Microscopy was performed at the Newcomb Imaging Center, Department of Botany, University of Wisconsin-Madison. EVWS was supported by Graduate Research Fellowship Program grant DGE-1747503. This material is based on work supported by the National Science Foundation under grant IOS-1552610 to PPS.

Appendix A. Supplementary data

Supplementary data to this article can be found online at https://doi.org/10.1016/j.ydbio.2021.02.006.

References

Akiyama-Oda, Y., Oda, H., 2006. Axis specification in the spider embryo: *dpp* is required for radial-to-axial symmetry transformation and *sog* for ventral patterning. Development 133, 2347–2357. https://doi.org/10.1242/dev.02400.

Akiyama-Oda, Y., Oda, H., 2020. Hedgehog signaling controls segmentation dynamics and diversity via *msx1* in a spider embryo. Science Advances 6, eaba7261. https://doi.org/10.1126/sciadv.aba7261.

Angelini, D., Kaufman, T., 2005. Functional analyses in the milkweed bug *Oncopeltus fasciatus* (Hemiptera) support a role for Wnt signaling in body segmentation but not appendage development. Dev. Biol. 283, 409–423. https://doi.org/10.1016/j.ydbio.2005.04.034.

Auman, T., Chipman, A.D., 2018. Growth zone segmentation in the milkweed bug *Oncopeltus fasciatus* sheds light on the evolution of insect segmentation. BMC Evol. Biol. 18, 178. https://doi.org/10.1186/s12862-018-1293-z.

Baig-Lewis, S., Peterson-Nedry, W., Wehrli, M., 2007. Wingless/Wnt signal transduction requires distinct initiation and amplification steps that both depend on Arrow/LRP. Dev. Biol. 306, 94–111. https://doi.org/10.1016/j.ydbio.2007.03.005.

Ballesteros, J.A., Sharma, P.P., 2019. A critical appraisal of the placement of xiphosura (Chelicerata) with account of known sources of phylogenetic error. Syst. Biol. 68, 896–917. https://doi.org/10.1093/sysbio/syz011.

Beermann, A., Pruhs, R., Lutz, R., Schroder, R., 2011. A context-dependent combination of Wnt receptors controls axis elongation and leg development in a short germ insect. Development 138, 2793–2805. https://doi.org/10.1242/dev.063644.

Benton, M.A., Pechmann, M., Frey, N., Stappert, D., Conrads, K.H., Chen, Y.-T., Stamataki, E., Pavlopoulos, A., Roth, S., 2016. Toll genes have an ancestral role in axis elongation. Curr. Biol. 26, 1609–1615. https://doi.org/10.1016/j.cub.2016.04.055.

Bolger, A.M., Lohse, M., Usadel, B., 2014. Trimmomatic: a flexible trimmer for Illumina sequence data. Bioinformatics 30, 2114–2120. https://doi.org/10.1093/bioinformatics/btu170.

Bolognesi, R., Beermann, A., Farzana, L., Wittkopp, N., Lutz, R., Balavoine, G., Brown, S.J., Schröder, R., 2008b. *Tribolium* Wnts: evidence for a larger repertoire in insects with overlapping expression patterns that suggest multiple redundant functions in embryogenesis. Dev. Gene. Evol. 218, 193–202. https://doi.org/10.1007/s00427-007-0170-3.

Bolognesi, R., Farzana, L., Fischer, T.D., Brown, S.J., 2008a. Multiple Wnt genes are required for segmentation in the short-germ embryo of *Tribolium castaneum*. Curr. Biol. 18, 1624–1629. https://doi.org/10.1016/j.cub.2008.09.057.

Bolognesi, R., Fischer, T.D., Brown, S.J., 2009. Loss of *Tc-arrow* and canonical Wnt signaling alters posterior morphology and pair-rule gene expression in the short-germ insect, *Tribolium castaneum*. Dev. Gene. Evol. 219, 369–375. https://doi.org/10.1007/s00427-009-0299-3.

Cadigan, K.M., Liu, Y.I., 2006. Wnt signaling: complexity at the surface. J. Cell Sci. 119, 395–402. https://doi.org/10.1242/jcs.02826.

Cadigan, K.M., Waterman, M.L., 2012. TCF/LEFs and Wnt signaling in the nucleus. CSH Perspect Biol 4, a007906. https://doi.org/10.1101/cshperspect.a007906 a007906.

Chawengsaksophak, K., de Graaff, W., Rossant, J., Deschamps, J., Beck, F., 2004. Cdx2 is essential for axial elongation in mouse development. Proc. Natl. Acad. Sci. U.S.A. 101, 7641–7645. https://doi.org/10.1073/pnas.0401654101.

Chesebro, J.E., Pueyo, J.I., Couso, J.P., 2013. Interplay between a Wnt-dependent organiser and the Notch segmentation clock regulates posterior development in *Periplaneta americana*. Biology Open 2, 227–237. https://doi.org/10.1242/bio.20123699.

Chipman, A.D., Arthur, W., Akam, M., 2004. A double segment periodicity underlies segment generation in centipede development. Curr. Biol. 14, 1250–1255. https://doi.org/10.1016/j.cub.2004.07.026.

Choe, C.P., Brown, S.J., 2009. Genetic regulation of *engrailed* and *wingless* in *Tribolium* segmentation and the evolution of pair-rule segmentation. Dev. Biol. 325, 482–491. https://doi.org/10.1016/j.ydbio.2008.10.037.

Cisne, J.L., 1974. Evolution of the world fauna of aquatic free-living arthropods. Evolution 28, 337–366.

Clark, E., 2017. Dynamic patterning by the *Drosophila* pair-rule network reconciles long-germ and short- germ segmentation. PLoS Biol. 15 (9), e2002439 https://doi.org/10.1371/journal.pbio.2002439.

Copf, T., Schröder, R., Averof, M., 2004. Ancestral role of caudal genes in axis elongation and segmentation. Proc. Natl. Acad. Sci. U.S.A. 101, 17711–17715. https://doi.org/10.1073/pnas.0407327102.

Damen, W.G.M., 2002. Parasegmental organization of the spider embryo implies that the parasegment is an evolutionary conserved entity in arthropod embryogenesis. Development 129, 1239–1250.

Damen, W.G.M., 2007. Evolutionary conservation and divergence of the segmentation process in arthropods. Dev. Dynam. 236, 1379–1391. https://doi.org/10.1002/dvdy.21157.

Damen, W., Weller, M., Tautz, D., 2000. Expression patterns of *hairy, even-skipped*, and *runt* in the spider *Cupiennius salei* imply that these genes were segmentation genes in a basal arthropod. Proc. Natl. Acad. Sci. U.S.A. 97, 4515–4519. https://doi.org/10.1073/pnas.97.9.4515.

Dearden, P.K., Akam, M., 2001. Early embryo patterning in the grasshopper, *Schistocerca gregaria: wingless, decapentaplegic* and *caudal* expression. Development 128, 3435–3444.

Donoughe, S., Extavour, C.G., 2016. Embryonic development of the cricket *Gryllus bimaculatus*. Dev. Biol. 411, 140–156. https://doi.org/10.1016/j.ydbio.2015.04.009.

Edgar, R.C., 2004. MUSCLE: multiple sequence alignment with high accuracy and high throughput. Nucleic Acids Res. 32, 1792–1797. https://doi.org/10.1093/nar/gkh340.

Ehrman, L.A., Yutzey, K.E., 2001. Anterior expression of the caudal homologue cCdx-B activates a posterior genetic program in avian embryos. Dev. Dynam. 221, 412–421. https://doi.org/10.1002/dvdy.1151.

El-Sherif, E., Zhu, X., Fu, J., Brown, S.J., 2014. Caudal regulates the spatiotemporal dynamics of pair-rule waves in *Tribolium*. PLoS Genet. 10, 13–e1004677. https://doi.org/10.1371/journal.pgen.1004677.

Fritzenwanker, J.H., Uhlinger, K.R., Gerhart, J., Silva, E., Lowe, C.J., 2019. Untangling posterior growth and segmentation by analyzing mechanisms of axis elongation in hemichordates. Proc. Natl. Acad. Sci. U.S.A. 116, 8403–8408. https://doi.org/10.1073/pnas.1817496116.

Hughes, C.L., Kaufman, T.C., 2002. Exploring Myriapod Segmentation: the expression patterns of *even-skipped, engrailed*, and *wingless* in a centipede. Dev. Biol. 247, 47–61. https://doi.org/10.1006/dbio.2002.0683.

Inoue, Y., Niwa, N., Mito, T., Ohuchi, H., Yoshioka, H., Noji, S., 2002. Expression patterns of *hedgehog, wingless*, and *decapentaplegic* during gut formation of *Gryllus bimaculatus* (cricket). Mech. Dev. 110, 245–248. https://doi.org/10.1016/s0925-4773(01)00584-6.

Isaacs, H.V., Pownall, M.E., Slack, J.M., 1998. Regulation of Hox gene expression and posterior development by the *Xenopus* caudal homologue Xcad3. EMBO J. 17, 3413–3427. https://doi.org/10.1093/emboj/17.12.3413.

Liu, P.Z., Kaufman, T.C., 2005. Short and long germ segmentation: unanswered questions in the evolution of a developmental mode. Evol. Dev. 7 (6), 629–646. https://doi.org/10.1111/j.1525-142X.2005.05066.

Logan, C.Y., Nusse, R., 2004. The Wnt signaling pathway in development and disease. Annu. Rev. Cell Dev. Biol. 20, 781–810. https://doi.org/10.1146/annurev.cellbio.20.010403.113126.

Love, M.I., Huber, W., Anders, S., 2014. Moderated estimation of fold change and dispersion for RNA-seq data with DESeq2. Genome Biol. 15, 21–31. https://doi.org/10.1186/s13059-014-0550-8.

Lybrand, D.B., Naiman, M., Laumann, J.M., Boardman, M., Petshow, S., Hansen, K., Scott, G., Wehrli, M., 2019. Destruction complex dynamics: Wnt/β-catenin signaling alters Axin-GSK3β interactions in in vivo. Development 146, dev164145. https://doi.org/10.1242/dev.164145.

Martin, B.L., Kimelman, D., 2009. Wnt signaling and the evolution of embryonic posterior development. Curr. Biol. 19, R215–R219. https://doi.org/10.1016/j.cub.2009.01.052.

Mcgregor, A.P., Pechmann, M., Schwager, E.E., Damen, W.G., 2009. An ancestral regulatory network for posterior development in arthropods. Commun. Integr. Biol. 2, 174–176. https://doi.org/10.4161/cib.7710.

Mcgregor, A.P., Pechmann, M., Schwager, E.E., Feitosa, N.M., Kruck, S., Aranda, M., Damen, W.G.M., 2008. *Wnt8* is required for growth-zone establishment and development of opisthosomal segments in a spider. Curr. Biol. 18, 1619–1623. https://doi.org/10.1016/j.cub.2008.08.045.

Mito, T., Kobayashi, C., Sarashina, I., Zhang, H., Shinahara, W., Miyawaki, K., Shinmyo, Y., Ohuchi, H., Noji, S., 2007. *even-skipped* has gap-like, pair-rule-like, and segmental functions in the cricket *Gryllus bimaculatus*, a basal, intermediate germ insect (Orthoptera). Dev. Biol. 303, 202–213. https://doi.org/10.1016/j.ydbio.2006.11.003.

Mittmann, B., Wolff, C., 2012. Embryonic development and staging of the cobweb spider *Parasteatoda tepidariorum* C. L. Koch, 1841 (syn.: *Achaearanea tepidariorum*; Araneomorphae; Theridiidae). Dev. Gene. Evol. 222, 189–216. https://doi.org/10.1007/s00427-012-0401-0.

Miyawaki, K., Mito, T., Sarashina, I., Zhang, H., Shinmyo, Y., Ohuchi, H., Noji, S., 2004. Involvement of Wingless/Armadillo signaling in the posterior sequential segmentation in the cricket, *Gryllus bimaculatus* (Orthoptera), as revealed by RNAi analysis. Mech. Dev. 121, 119–130. https://doi.org/10.1016/j.mod.2004.01.002.

O'Donnell, B.C., Jockusch, E.L., 2010. The expression of *wingless* and Engrailed in developing embryos of the mayfly *Ephoron leukon* (Ephemeroptera: polymitarcyidae). Dev. Gene. Evol. 220, 11–24. https://doi.org/10.1007/s00427-010-0324-6.

Ober, K.A., Jockusch, E.L., 2006. The roles of wingless and decapentaplegic in axis and appendage development in the red flour beetle, *Tribolium castaneum*. Dev. Biol. 294, 391–405. https://doi.org/10.1016/j.ydbio.2006.02.053.

Oda, H., Nishimura, O., Hirao, Y., Tarui, H., Agata, K., Akiyama-Oda, Y., 2007. Progressive activation of Delta-Notch signaling from around the blastopore is required to set up a functional caudal lobe in the spider *Achaearanea tepidariorum*. Development 134, 2195–2205. https://doi.org/10.1242/dev.004598.

Paese, C.L.B., Schoenauer, A., Leite, D.J., Russell, S., Mcgregor, A.P., 2018. A SoxB gene acts as an anterior gap gene and regulates posterior segment addition in a spider. Elife 7, e37567. https://doi.org/10.7554/eLife.37567.

Panfilio, K.A., Vargas Jentzsch, I.M., Benoit, J.B., Erezyilmaz, D., Suzuki, Y., Colella, S., Robertson, H.M., Poelchau, M.F., Waterhouse, R.M., Ioannidis, P., et al., 2019. Molecular evolutionary trends and feeding ecology diversification in the Hemiptera, anchored by the milkweed bug genome. Genome Biol. 20, 64. https://doi.org/10.1186/s13059-019-1660-0.

Patro, R., Duggal, G., Love, M.I., Irizarry, R.A., Kingsford, C., 2017. Salmon provides fast and bias-aware quantification of transcript expression. Nat. Methods 14, 417–419. https://doi.org/10.1038/nmeth.4197.

Pechmann, M., Benton, M.A., Kenny, N.J., Posnien, N., Roth, S., 2017. A novel role for *Ets4* in axis specification and cell migration in the spider *Parasteatoda tepidariorum*. Elife 6, e27590. https://doi.org/10.7554/eLife.27590.001.

Pechmann, M., Khadjeh, S., Turetzek, N., Mcgregor, A.P., Damen, W.G.M., Prpic, N.-M., 2011. Novel function of Distal-less as a gap gene during spider segmentation. PLoS Genet. 7, e1002342 https://doi.org/10.1371/journal.pgen.1002342.

Pechmann, M., Mcgregor, A.P., Schwager, E.E., Feitosa, N.M., Damen, W.G.M., 2009. Dynamic gene expression is required for anterior regionalization in a spider. Proc. Natl. Acad. Sci. U.S.A. 106, 1468–1472. https://doi.org/10.1073/pnas.0811150106.

Peterson-Nedry, W., Erdeniz, N., Kremer, S., Yu, J., Baig-Lewis, S., Wehrli, M., 2008. Unexpectedly robust assembly of the Axin destruction complex regulates Wnt/Wg signaling in Drosophila as revealed by analysis in vivo. Dev. Biol. 320, 226–241. https://doi.org/10.1016/j.ydbio.2008.05.521.

Pinson, K.I., Brennan, J., Monkley, S., Avery, B.J., Skarnes, W.C., 2000. An LDL-receptor-related protein mediates Wnt signalling in mice. Nature 407, 535–538. https://doi.org/10.1038/35035124.

Refki, P.N., Khila, A., 2015. Key patterning genes contribute to leg elongation in water striders. EvoDevo 6, 14. https://doi.org/10.1186/s13227-015-0015-5.

Rueden, C.T., Schindelin, J., Hiner, M.C., DeZonia, B.E., Walter, A.E., Arena, E.T., Eliceiri, K.W., 2017. ImageJ2: ImageJ for the next generation of scientific image data. BMC Bioinf. 18, 529. https://doi.org/10.1186/s12859-017-1934-z.

Schindelin, J., Arganda-Carreras, I., Frise, E., Kaynig, V., Longair, M., Pietzsch, T., Preibisch, S., Rueden, C., Saalfeld, S., Schmid, B., Tinevez, J.-Y., White, D.J., Hartenstein, V., Eliceiri, K., Tomancak, P., Cardona, A., 2012. Fiji: an open-source platform for biological-image analysis. Nat. Methods 9, 676–682. https://doi.org/10.1038/nmeth.2019.

Schönauer, A., Paese, C.L.B., Hilbrant, M., Leite, D.J., Schwager, E.E., Feitosa, N.M., Eibner, C., Damen, W.G.M., Mcgregor, A.P., 2016. The Wnt and Delta-Notch signalling pathways interact to direct pair-rule gene expression via caudal during segment addition in the spider *Parasteatoda tepidariorum*. Development 143, 2455–2463. https://doi.org/10.1242/dev.131656.

Schoppmeier, M., Damen, W.G.M., 2005. *Suppressor of Hairless* and *Presenilin* phenotypes imply involvement of canonical Notch-signalling in segmentation of the spider *Cupiennius salei*. Dev. Biol. 280, 211–224. https://doi.org/10.1016/j.ydbio.2005.01.024.

Setton, E.V.W., March, L.E., Nolan, E.D., Jones, T.E., Cho, H., Wheeler, W.C., Extavour, C.G., Sharma, P.P., 2017. Expression and function of *spineless* orthologs correlate with distal deutocerebral appendage morphology across Arthropoda. Dev. Biol. 430, 224–236. https://doi.org/10.1016/j.ydbio.2017.07.016.

Setton, E.V.W., Sharma, P.P., 2018. Cooption of an appendage-patterning gene cassette in the head segmentation of arachnids. Proc. Natl. Acad. Sci. U.S.A. 115, E3491–E3500. https://doi.org/10.1073/pnas.1720193115.

Schwager, E.E., Meng, Y., Extavour, C.G., 2015. *Vasa* and *piwi* are required for mitotic integrity in early embryogenesis in the spider *Parasteatoda tepidariorum*. Dev. Biol. 402, 276–290. https://doi.org/10.1016/j.ydbio.2014.08.032.

Schwager, E.E., Pechmann, M., Feitosa, N.M., Mcgregor, A.P., Damen, W.G.M., 2009. *Hunchback* functions as a segmentation gene in the spider *Achaearanea tepidariorum*. Curr. Biol. 19, 1333–1340. https://doi.org/10.1016/j.cub.2009.06.061.

Schwager, E.E., Sharma, P.P., Clarke, T., Leite, D.J., Wierschin, T., Pechmann, M., Akiyama-Oda, Y., Esposito, L., Bechsgaard, J., Bilde, T., et al., 2017. The house spider genome reveals an ancient whole-genome duplication during arachnid evolution. BMC Biol. 15, 62. https://doi.org/10.1186/s12915-017-0399-x.

Sharma, P.P., Kaluziak, S.T., Perez-Porro, A.R., Gonzalez, V.L., Hormiga, G., Wheeler, W.C., Giribet, G., 2014. Phylogenomic interrogation of Arachnida reveals systemic conflicts in phylogenetic signal. Mol. Biol. Evol. 31, 2963–2984. https://doi.org/10.1093/molbev/msu235.

Shimizu, T., Bae, Y.-K., Muraoka, O., Hibi, M., 2005. Interaction of Wnt and caudal-related genes in zebrafish posterior body formation. Dev. Biol. 279, 125–141. https://doi.org/10.1016/j.ydbio.2004.12.007.

Shinmyo, Y., Mito, T., Matsushita, T., Sarashina, I., Miyawaki, K., Ohuchi, H., Noji, S., 2005. *Caudal* is required for gnathal and thoracic patterning and for posterior elongation in the intermediate-germband cricket *Gryllus bimaculatus*. Mech. Dev. 122, 231–239. https://doi.org/10.1016/j.mod.2004.10.001.

Stamatakis, A., 2014. RAxML version 8: a tool for phylogenetic analysis and post-analysis of large phylogenies. Bioinformatics 30, 1312–1313. https://doi.org/10.1093/bioinformatics/btu033.

Stollewerk, A., Schoppmeier, M., Damen, W.G.M., 2003. Involvement of *Notch* and *Delta* genes in spider segmentation. Nature 423, 863–865. https://doi.org/10.1038/nature01682.

Tolwinski, N.S., Wehrli, M., Rives, A., Erdeniz, N., DiNardo, S., Wieschaus, E., 2003. Wg/wnt signal can Be transmitted through arrow/LRP5,6 and axin independently of Zw3/Gsk3β activity. Dev. Cell 4, 407–418. https://doi.org/10.1016/S1534-5807(03)00063-7.

van den Akker, E., Forlani, S., Chawengsaksophak, K., de Graaff, W., Beck, F., Meyer, B.I., Deschamps, J., 2002. Cdx1 and Cdx2 have overlapping functions in anteroposterior patterning and posterior axis elongation. Development 129, 2181–2193.

Wehrli, M., Dougan, S.T., Caldwell, K., O'Keefe, L., Schwartz, S., Vaizel-Ohayon, D., Schejter, E., Tomlinson, A., DiNardo, S., 2000. *Arrow* encodes an LDL-receptor-related protein essential for Wingless signalling. Nature 407, 527–530. https://doi.org/10.1038/35035110.

Zeng, V., Extavour, C.G., 2012. ASGARD: an open-access database of annotated transcriptomes for emerging model arthropod species. Database 2012, bas048. https://doi.org/10.1093/database/bas048.

Zeng, X., Huang, H., Tamai, K., Zhang, X., Harada, Y., Yokota, C., Almeida, K., Wang, J., Doble, B., Woodgett, J., et al., 2007. Initiation of Wnt signaling: control of Wnt coreceptor Lrp6 phosphorylation/activation via frizzled, dishevelled and axin functions. Development 135, 367–375. https://doi.org/10.1242/dev.013540.